TÉCNICO LISBOA

Experimental characterization of the flow and heat transfer inside a horizontal circular tube using C_{60}/tetralin nanofluid

Rita Adrião Lamosa

Thesis to obtain the Master of Science Degree in

Mechanical Engineering

Supervisor(s): Dr. Ana Sofia Oliveira Henriques Moita
Prof. Antonio Luis Nobre Moreira

Examination Committee

Chairperson: Prof. Edgar Caetano Fernandes
Supervisor: Dr. Ana Sofia Oliveira Henriques Moita
Member of the Committee: Prof. Helder Manuel Ferreira dos Santos

November 2019

Dedicated to my parents.

Acknowledgments

A few words about the most important people during these last years studying in *Instituto Superior Técnico*, and, specially, in the development of this thesis.

First of all, I would like to thank to Dr. Ana Moita, my supervisor, for all her dedication, support, suggestions and writing revisions. Then, to the post-doctoral researcher Artem Nikulin, for all of the time devoted helping me, with all of his precious explanations. And also, a thank you to professor Antonio Moreira for giving me the opportunity to work in IN+.

Besides I would like to thank to all my colleagues and friends that I made during these years, for the amazing moments and experiences that I will never forget.

A thank you to all my friends from the Spanish School, those amazing guys that are my second family, for all of the support and encouragement throughout my years of study.

Finally to my family, and specially, to my parents, two wonderful people that made me who I am.

Thank you.

Resumo

Nesta dissertação foi estudado o comportamento hidrodinâmico e a transferência de calor em regime laminar, transição e turbulento do nanofluido C_{60}/tetralin, dentro de um tubo, horizontal e circular, com 3.5 mm de diâmetro interno, com um fluxo de calor imposto na superfície. Foram experimentalmente testadas três concentrações diferentes do nanofluido (0.10%, 0.30% e 0.66% em massa) e tetralin puro a diferentes caudais mássicos e a temperaturas de entrada diferentes (25º, 35º e 45ºC). Os valores obtidos de temperatura e pressão permitiram o cálculo dos fatores de atrito e dos coeficientes de transferência de calor por convecção. Os resultados permitiram concluir que, à medida que a temperatura aumenta, o fator de atrito aumenta com o aumento da concentração em massa das partículas, o que representa um aumento da potência de bombeamento requerida. Por outro lado, também permitiram concluir que o coeficiente de transferência de calor melhora quando avaliado em função do número de Reynolds. No entanto, quando avaliado à mesma velocidade do escoamento, os resultados mostram uma diminuição do coeficiente de transferência de calor para o nanofluido de maior concentração de partículas, 0.66% em massa. Este efeito da adição das nanopartículas foi atribuído à diminuição de intensidade da turbulência e ao aumento da viscosidade dos nanofluidos.

Palavras-chave: Nanofluidos, Concentração das nanopartículas, Temperatura, Fator de atrito, Coeficiente de transferência de calor por convecção, Regime de transição.

Abstract

In this thesis, the hydrodynamic behavior and the heat transfer of C_{60}/tetralin nanofluid is investigated in a horizontal, circular, smooth, mini-tube with 3.5 mm of inner diameter, under an imposed constant heat flux, for laminar, transition and turbulent flow regimes. Three mass concentrations of nanofluid (0.10%, 0.30% and 0.66 mass%) as well as pure tetralin were experimentally tested at different mass flow rates and at three different inlet temperatures (25º, 35º and 45ºC). Temperature and pressure drop measurements were taken, allowing to determine friction factors and convective heat transfer coefficients. It was found that, with temperature raise, the friction factor increased with the mass concentration of the nanoparticles, which represents a penalty on the pumping power. The results also show that the convective heat transfer coefficient was enhanced when comparing data from heat transfer coefficient values plotted against the Reynolds number. However, when comparing the heat transfer coefficients for the same velocity of the flow, the results show a decrease in the heat transfer coefficient value for the 0.66 mass% nanofluid. This effect of the addition of C_{60} nanoparticles was attributed to the decrease of turbulence intensity as well as to the increased viscosity of the nanofluids.

Keywords: Nanofluid, Nanoparticles concentration, Temperature, Friction factor, Convective heat transfer coefficient, Transition flow regime.

Contents

List of Tables

List of Figures

Nomenclature

Symbols

$\dot{m}$	Mass flow rate [kg/s]
$\overline{T}$	Mean temperature [ºC]
Cp	Specific heat capacity [J/(kg· K)]
D	Tube inner diameter [m]
f	Friction factor [-]
Gr	Grashof number [-]
h	Heat transfer coefficient [W/(m^2· K)]
I	Electrical current [A]
j	Colburn j-factor [-]
k	Thermal conductivity [W/(m· K)]
L	Tube length [m]
m	Mass [kg]
Nu	Nusselt number [-]
Pr	Prandtl number [-]
q	Thermal power [W]
q''	Heat flux [W/m^2]
Re	Reynolds number [-]
Ri	Richardson number [-]
T	Temperature [ºC]
U	Fluid mean velocity [m/s]
V	Voltage [V]

w Particle mass fraction [%]

x Axial position [m]

Greek symbols

α Thermal diffusivity [m^2/s]

β Thermal expansion coefficient [k^{-1}]

ΔP Pressure drop [Pa]

ΔT Temperature difference [°C]

$\dot{\gamma}$ Shear rate [1/s]

μ Dynamic viscosity [(N· s)/m^2]

ν Kinematic viscosity [m^2/s]

ϕ Particle volume fraction [%]

ρ Density [kg/m^3]

τ Shear stress [Pa]

Subscripts

bf Base fluid

crt Critical

fd,h Fully developed hydrodynamically

fd,t Fully developed thermally

i Inlet

lam Laminar

np Nanoparticles

o Outlet

s Surface

tr Transition

$turb$ Turbulent

Chapter 1

Introduction

1.1 Motivation and overview

In the last few decades environmental concerns have been growing. Human activity with its over-exploration of resources is one of the main causes.

The increase in primary energy consumption is mainly dependent on the consumption of fossil fuels. These fuels are the principal responsible for the emission of some of the gases causing greenhouse effect, such as CO_2.

Due to this, automobile industry has been searching for alternative methods to improve the efficiency of internal combustion engines (ICE). In this kind of engine a large portion of the fuel energy (about 40 percent) is lost in the exhaust system. In order to use this energy with the objective of reducing the CO_2 emissions and improving the thermal efficiency, several waste heat recovery (WHR) systems have been proposed. One of them uses the Rankine Cycle, a cycle based on the steam generation in a secondary circuit.

The most important element in the Rankine Cycle is the heat exchanger (HX), which must be as efficient and compact as possible, since an enhancement of its performance can contribute to a reduction of energy consumption. A heat exchanger is a system widely used in engineering applications that allows the transfer of heat between two or more fluids. There are different possible configurations, the one to be implemented in the application which motivated the present work is a cross flow tube heat exchanger (figure 1.1) with the working fluid circulating inside the tubes and the exhaust gases circulating in the exterior [2]. Some work has been already developed in previous works that contributed to the development of this heat exchanger. So, while Santos and co authors have worked on the implementation and test of whole Rankine cycle based waste recovery system [1–3], Andrade [4] focused on a more fundamental study, addressing the pressure drop and heat transfer in a flow inside smooth and corrugated tubes.

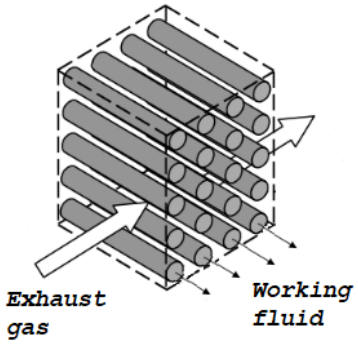

Figure 1.1: Cross flow HX (adapted from [1]).

The present thesis is in line with this project and intends to further improve the heat transfer in the heat exchanger, not by changing the surface properties, but now acting on the properties of the working fluid, by testing it under working conditions closer to those of the real operating heat waste recovery system, being the general working fluid temperatures in the range of 30º to 350ºC [1].

It is well known that one of the main limitations in the development of energy-efficient heat transfer medium is the low thermal conductivity of the conventional fluids, such as water or oil [5]. To overcome this issue, several authors suggest the use of nanofluids, i.e. colloidal mixtures of nano-sized particles in a base fluid. This new type of fluid has heat transfer characteristics superior to both of the base fluid and suspend particles. It offers a compact, green approach when high thermal loads are in demand, having many potential applications in an engineering point of view [6]. A substantial increase in liquid thermal conductivity, heat capacity and heat transfer coefficients are currently reported in the literature when using nanofluids (Murshed et al. [7], Li and Xuan [8]). However, an increase in nanoparticles concentration is also known to often increase the viscosity of the bulk solution, which can lead to several issues related to the fluid flow and to pressure losses [5, 9]. This thesis explores the effect of nanoparticles concentration to infer on the counter effects of heat transfer improvement versus increase in the pressure losses, to evaluate their effectiveness to effectively improve the heat transfer in internal flows in mini-tubes, in the context of the heat transfer enhancement of the aforementioned heat exchanger.

Other applicability of the study developed in this thesis is the possible use of the nanofluid in a solar energy system. As explained in the previous paragraphs, with global warming, there is an increasing need for the use of clean and renewable energy sources and energy conversion systems. One of the main types of renewable energy sources is solar energy, which has been receiving substantial attention of researchers in the last few decades. There are two methods to produce electricity using solar energy, namely the solar thermal power plants and photovoltaic (PV) systems. In the first one the energy from the sun is used to heat a working fluid, which is then used to run a turbine in a power plant. This mechanical energy is than converted into electricity by a generator. These systems use solar collectors, i.e. sun facing surfaces that absorb solar energy and transfer it to the working fluid. In the case of the PV system the sunlight is directly used to generate electricity. However, when using photovoltaic systems, only around 12 to 20% of the sunlight is converted into electricity, while the remaining energy is dissipated in the form of heat, thus increasing the temperature of the photovoltaic cells and consequently decreasing their efficiency [10]. Combining the two methods allows to produce electrical and thermal energy simultaneously, in a system called photovoltaic thermal (PVT) system. This consists in a PV module and a heat extraction part which cools the PV module, thus allowing it to achieve higher efficiencies than conventional PV systems.

In the context of enhancing PV systems efficiency, an alternative technology that has been explored with the purpose of improving the performance and reducing the cost of PV panels, are solar concentrators. The concentration of solar radiation on the PV cells surface increases the electrical energy output, which makes the system to be more economic. The increase of the illumination intensity in the panel surface will increase the solar panel efficiency. Also, it allows to reduce PV panel area, which is highly expensive, by only adding cheaper lenses or mirrors. However, this method increases the PV cell tem-

perature problem. As the temperature raises, the efficiency of the PV cells drops and, in long term, the excess temperatures cause irreversible damages to the cells [11]. Therefore, an efficient cooling system is a paramount element to keep the operating temperature below a given limit.

There are many cooling methods such as the heat pipe technique or the water cooling method [12, 13]. Odeh and Behnia [14] studied the water cooling system under different weather conditions and concluded that when using this technique the system output increased in the range of 4 to 10%.

Given that the use of the extracted thermal energy, from cooling, can increase the efficiency of the receiver, it is desirable that the working fluid of the cooling system transfer as much heat as possible. For a PVT system [15] the outlet working fluid temperature is in the range of 60º to 80ºC. Also, for converting solar energy into thermal energy, in the solar collectors, an efficient heat transfer between the media is required. The common working fluids used are water, oil and ethylene glycol, which are not much efficient due to their low values of thermal conductivity. So, in both cases, the use of a fluid with higher thermal conductivity is desirable, being nanofluids an excellent option. The applicability of nanofluids in solar energy systems has been studied in the last few years, as reviewed for instance by Kasaeian et al. [16] and Wahab et al. [17].

Despite of their potential advantages, the use of nanofluids has not been generalized for industrial applications yet. One of the main issues is the high cost of the materials and of the preparation techniques required. Also, stability of the prepared solutions is an important issue, as the nanoparticles often tend to agglomerate and/or deposit, causing large heterogeneity in the properties of the bulk fluid and often precluding the use of the nanofluid [5]. On the other hand, it is known that increasing the concentration of the nanoparticles often leads to a significant increase of the nanofluid viscosity, with consequent increase of the friction factor and pressure losses [9]. Hence the ”optimum” nanoparticles concentration must be found to balance the potential benefits of improving the thermal properties of the base fluid, while controlling the penalty of an increased viscosity of the resulting nanofluid.

In the present study the nanofluid used is a mixture of fullerene particles, C_{60}, and tetralin. Fullerene is an allotrope of Carbon, one of the many forms that carbon based materials can assume. It is a substance produced naturally, in small quantities, that was discovered in 1985 by Kroto et al. [18], being the Buckminsterfullerene (C_{60}) the most common form to find. Fullerenes form a unique molecular structure with rigid, well-defined geometries. This structure is very resistant but the molecular bond is quite weak due to weak Van der Waals forces. Carbon nanostructures have been used for nanofluids due to their properties, being in the category of the best materials to use in nanofluids. Many of these superior properties are related to the very high symmetry of the C_{60} molecule. The 60 carbon atoms are located at the vertices of a truncated icosahedron, being this the most spherical molecule known [19]. Its unique cage structure allows an interesting interaction with solvents, having the capability of dissolving in common organic solvents. Since this is the only carbon species with this characteristic, it is a substance widely used [20, 21].

Tetralin, (1,2,3,4-Tetrahydronaphthalene) is a hydrocarbon. It consists entirely in carbon and hydrogen, having the chemical formula of $C_{10}H_{12}$. It is a colorless liquid, with a strong moldy smell. This substance is obtained from the catalytic hydrogenation of the naphthalene, being the primary or inter-

mediate result, as showed in Rautanen et al. [22]. Tetralin has been widely used in coal liquefaction [23, 24], but also, with the increasing environmental concern, in liquefaction of biomass to obtain clean bio-fuels [25]. Also tetralin is a substance relatively cheap, with an average cost of 8 US dollars per kilogram [26].

Other important use of tetralin, which is more in line with the current study, was its application as heat transfer fluid in nuclear power energy, as a coolant. With the objective of expand globally the use of nuclear energy many research and development programs have been carried out, Chikazawa et al. [27]. One of them was the Sodium Reactor Experiment. This consists in a sodium-cooled thermal reactor operating in Santa Susana Field Laboratory, USA. This reactor operated from 1957 to 1964 and had an electrical output of 5.8 MW. In this power plant, tetralin was used to cool the primary pump seals.

C_{60} particles have a very good solubility in tetralin, which further improve as the fluid temperature increases, as explained in Kozlov et al. [28]. Fullerene particles are very easy to mix with tetralin, forming a stable mixture. Since the stability of the nanofluid is one of the most difficult obstacles to overcome when preparing a nanofluid, as aforementioned and given it's high potential to be used in heat transfer applications, at reduced costs, as demonstrated in the nuclear power plants cooling studies also cited before, tetralin based nanofluids using fullerene nanoparticles are the main nanofluids which were used in the present work.

1.2 Objectives

In the context of the motivation described in the previous paragraphs, this thesis is integrated in a broader project addressing the development and test of a compact and efficient heat exchanger. This heat exchanger is to be included in different applications requiring the dissipation of high heat loads, being the main focus in a Rankine cycle waste recovery system to be implemented in heavy duty vehicles and in cooling systems for concentrated photovoltaic panels.

So, the goal of this work is to contribute to that major objective, studying the potential to improve the properties of the working fluid. In this context, the main objective is to evaluate the potential use of nanofluids as working fluid, inferring on the potential advantage of the enhanced thermal properties of such fluids with the possible disadvantage of increased pressure losses due to the increase in viscosity.

To achieve this goal this study addresses the experimental characterization of pure tetralin and tetralin based solutions mixed with fullerene nanoparticles at three different mass concentrations, namely 0.10%, 0.30% and 0.66%. To do so, these fluids were tested in an experimental setup with a horizontal, circular, smooth tube. The experimental conditions are varied to cover a wide range of flow regimes, from laminar to turbulent, allowing to analyze the transition flow regime. The surface of the tube is heated with an imposed constant heat flux.

1.3 Thesis Outline

This thesis is divided in five chapters. The introduction explain the context and motivation of this work, briefly discussing the applicability of nanofluids, as well as the characteristics of tetralin and fullerene particles (C_{60}) used. This introductory chapter also establishes the main objective of the present study.

In the second chapter a bibliographic review is presented, while introducing the most important concepts and theoretical background that are required to understand the experimental methods and the results, described and discussed in the following chapters. So, fluid dynamic and heat transfer concepts in an internal flow are firstly introduced. Then, a review on nanofluids is addressed focusing on their most relevant characteristics and their preparation. This review also includes a number of studies focusing the applicability of nanofluids in internal flows, stressing their advantages and limitations to overcome.

The third chapter addresses the detailed description of the experimental setup used and the procedures followed. This chapter also explains the preparation and characterization of the nanofluids, a major part of the current work. Finally, a last sub-section describes the data processing and the uncertainty analyses.

The results obtained experimentally are presented and discussed in the forth chapter. The first results are used to validate the experimental setup and evaluated the thermal losses. Then the flow is characterized in detail, both from the hydrodynamic and thermal point of view. Main emphasis in the analysis and interpretation of the results is put on the main effects of the nanoparticles concentration and how they affect the thermal and the hydrodynamic behavior of the flow in the various flow regimes, from the laminar to the turbulent regime. The applicability and limitations of the correlations presented in the literature to the nanofluids is also discussed to stress the main effects of the nanoparticles that must be included in those correlations.

Finally the fifth chapter summarizes the main conclusions of this work and suggests several topics and activities to be developed as future work.

Chapter 2

Background

2.1 Internal flow

In contrast to an external flow, such as a parallel flow over a flat plate, in an internal flow such as a flow in a pipe, the fluid is constrained to a space. The boundary layer can not develop freely; instead it develops until the constrain. Three main regimes can be identified in the internal flow, namely the laminar, the transition and the turbulent flow, which are determined based on the value of the Reynolds number:

$$Re = \frac{4\dot{m}}{\mu\pi D} \tag{2.1}$$

where $\dot{m}$ is the mass flow rate inside the tube, D is the tube inner diameter and μ is the dynamic viscosity of the fluid, being this form of the Reynolds number only valid for circular tubes.

The Reynolds number is a dimensionless quantity that represents the ratio between inertia and viscous forces. This means that, for low values of the Reynolds number, the inertia forces are insignificant relatively to viscous forces. It represents the laminar region, where the flow is highly ordered. As the Reynolds number increases, the inertia forces also increase, some disturbances emerge causing the instability of the boundary layer and transitional flow regime takes place. In this regime, turbulent eddies occur, being the flow unstable and chaotic. Since the Moody diagram development [29] it is known that the transition takes place in some space interval, being the critical Reynolds, at x_{crt}, the beginning of this regime, $x_{crt} \leq x_{tr} \leq x$. Little information is available for this region separating laminar and turbulent flow, so, in many cases, it is reduced to a point ($Re_{crt} \approx Re_{tr}$). This point is represented by the critical Reynolds, that, in fully developed flow is $Re_{ct} \approx 2300$ [30]. As the Reynolds number increases the intensity of the turbulence also increases, being necessary a value of $Re \approx 10000$ to achieve fully turbulent conditions.

The transition between laminar and turbulent flow is a complex phenomenon and its physics and implications are not fully understood. Due to the little information available in the literature and its uncertainty it is a usually advised when designing heat exchangers to avoid this flow regime. However, according to Meyer and Olivier [31], the best compromised between high heat transfer and low pressure

drop is close to this flow regime and in practice, many heat exchangers in industrial applications actually work under transition regime conditions. That is the main goal of the designers, since as the pressure drop raises, higher pumping power is required, which represents higher operational costs. It is known that in the laminar flow the heat transfer and the pressure drop are both low, while in the turbulent flow regime the heat transfer coefficients are higher but also the pressure drop. That is why many heat exchangers operate in, or close, to the transitional flow regime [31].

The transition flow regime has been mainly studied by two main research groups [29, 32]. One of them is the group of Afshin Ghajar and co-workers from Oklahoma State University, who published more than 30 studies on experimental work in this regime. They investigated the effect of different types of inlets on pressure drop and heat transfer in smooth tubes. The beginning and end of transition was observed to be strongly affected by the inlet geometry, being delayed for smoother inlet geometries and for increasing heat flux. In the laminar region the heat transfer coefficient and the friction coefficient increased as the heat flux increased, being influenced by secondary flow effects. However, in the turbulent region no changes occurred, being the coefficients independent of the inlet geometry, heat flux and secondary flow.

The other research group focusing on the transition flow regime is the working group of Professor Josua Meyer, from the University of Pretoria. Their experiments were mainly conducted with constant wall temperature and the test fluid was being cooled and not heated as in Ghajar's work, although they also conducted experiments with constant heat flux condition. Meyer and co-authors studied different inlet geometries in smooth and in enhanced tubes. They also addressed nanofluids [33–37].

This thesis is focused on the heat transfer between the fluid (nanofluid) and the smooth circular tube where it circulates. This heat transfer mode is called convection, and it consists in the energy transfer between a surface and a moving fluid over this surface when they are at different temperatures. There are two types of convection, forced convection and free convection, being mixed convection when the two modes of convection are present. Convection in horizontal tubes has been studied for several decades, starting with earlier works such as that of Shannon and Depew [38] in 1968, who investigated the influence of forced and free convection in water. In forced convection the motion of the fluid is induced by and external force, such as a pump. Natural or free convection occurs in the absence of an external force. When heat is applied to the wall, a temperature gradient of the fluid leads to density differences between the wall and the pipe center, as the density is dependent of the temperature, generally decreasing with increasing in temperature. This density gradient and the presence of a body force (gravity) cause buoyancy effects, leading to free convection. Especially in horizontal tubes, the buoyancy forces may induce a secondary flow which increases the heat transfer between the fluid and the wall. Free convection also increases pressure drop, reduces thermal entrance length and induces an early transition to turbulent flow as explain in [39].

There are some methods to identify the convection type in fluid, such as flow regime maps and peripheral heat transfer ratio [40]. The one used here is the Richardson number method,

$$Ri = \frac{Gr}{Re^2} \tag{2.2}$$

where Gr is the Grashof number and represents a measure of the ratio of buoyancy forces to viscous forces. So, as Richardson number increases, the buoyancy forces also increase until free convection dominates the flow. For $Ri < 0.1$ free convection is negligible, so the flow is in pure forced convection. For $0.1 \leq Ri \leq 10$ both convection are present in the flow, so that mixed convection is assumed. In case $Ri > 10$ the flow is treated as free convection.

2.1.1 Hydrodynamic considerations

The boundary layer concept can be explained considering the case of a parallel flow over a flat plate. The particles of the flow in contact with the plate surface have zero velocity and delay the motion of the particles in the adjoining layer of the fluid. This retardation of the fluid motion proceed until the distance $y = \delta$, representing δ the boundary layer thickness, usually defined as the distance where the velocity of the flow is 99% of the velocity outside the boundary layer (u_∞), $U = 0.99u_\infty$.

In the case of an internal flow, when the fluid enters the tube with uniform velocity, a velocity boundary layer also develops in the tube wall, but in this case it is constrained to a space, developing until the boundary layers intercept each other in the centerline. Figure 2.1 represents a laminar flow inside a round tube. This figure allows to observe the evolution of the velocity profile along the hydrodynamic development of the boundary layer.

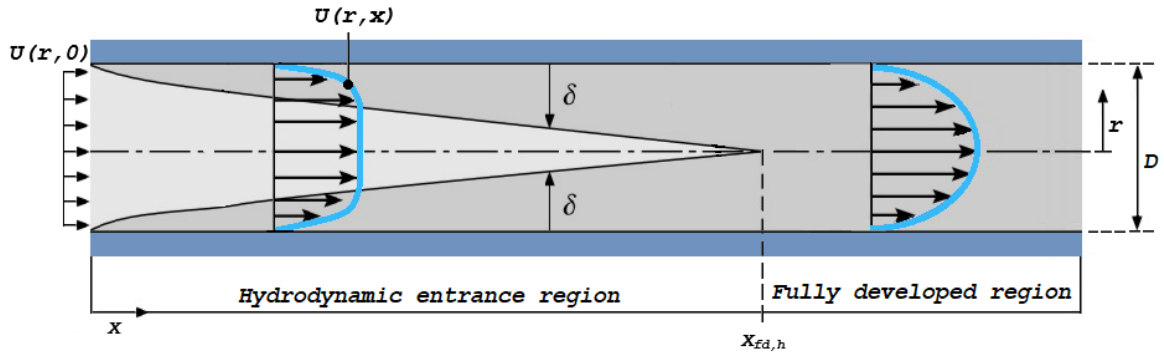

Figure 2.1: Hydrodynamic boundary layer development in a circular tube (adapted from [30]).

The distance the flow run until the boundary layers intercept each other in the centerline and the velocity profile stabilizes is called the hydrodynamic entry length. This length is determined by the follow equations:

$$x_{fd,h_{lam}} = 0.05ReD \tag{2.3}$$

$$10D \leq x_{fd,h_{turb}} \leq 60D \tag{2.4}$$

being $x_{fd,h_{lam}}$ valid for laminar flow, $Re \leq 2300$, and $x_{fd,h_{turb}}$ for turbulent flow, $Re > 2300$. After this length the flow is assumed to be fully developed. In this region the velocity profile no longer changes, depicting, for a laminar flow inside a tube, a parabolic profile, as illustrated in 2.1.

Pressure gradient

One of the more important factors from an industrial/engineering point of view is the pressure drop. This parameter determines the power requirements, namely pump power, to keep the internal flow. The aim is to have the minimum possible pressure drop due to the elevated cost of this kind of operations, as explained before. The pressure drop of the flow inside a tube is usually evaluated based on the calculation of the friction factor, which is a dimensionless parameter that can be determined by the Darcy-Weisbach equation:

$$f = \frac{2D\Delta P}{\rho L U^2} \tag{2.5}$$

where ΔP is the pressure drop along the test section; ρ is the density of the working fluid; U is the velocity; L is the length between pressure sensors and D is the inner diameter of the tube. There are several correlations to describe the friction factor in a circular tube. For the laminar flow, equation 2.5 can be reduced to the well-known Hagen-Poiseuille equation:

$$f = \frac{64}{Re} \tag{2.6}$$

For the turbulent flow, one of the most used equations to calculate the friction factor in a smooth tube is the Blasius equation:

$$f = 0.316 Re^{-1/4} \tag{2.7}$$

only valid for $Re \leq 2 \cdot 10^4$.

2.1.2 Thermal considerations

As well as the velocity boundary layer develops, the thermal boundary layer must also develop if the fluid flow and the surface have different temperatures. In this case, the particles exchange energy and a temperature gradient grow in the fluid. δ_t is the thermal boundary layer thickness and is usually defined as the distance for which $(T_s - T)(T_s - T_\infty) = 0.99$, where T_s is the surface temperature, T is the temperature of the fluid and T_∞ is the temperature outside the boundary layer.

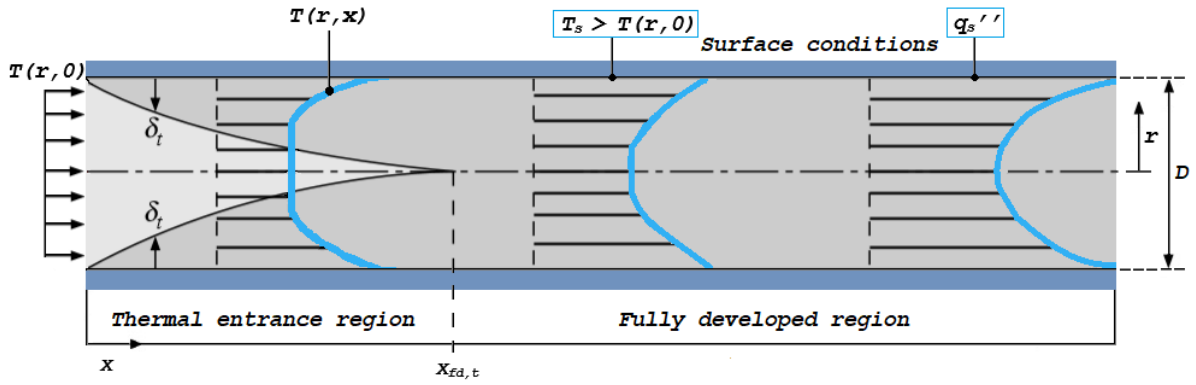

Figure 2.2: Thermal boundary layer development in a circular tube (adapted from [30]).

Figure 2.2 represents the thermal boundary layer development in a circular tube. In the internal flow,

the fluid enters with a uniform temperature $T(r,0)$ and since the tube wall has a higher temperature, convection heat transfer takes place and the thermal boundary layer develops. There are two ways to maintain the surface boundary condition, namely by imposing a uniform temperature or a uniform heat flux. In both ways the fully developed region will be achieved after the thermal entrance region. The thermal entrance length is an important aspect for design engineers. It determines if the heat transfer coefficient is dependent (developing flow) or independent (fully developed flow) from the axial position. This length is determined by the follow equations:

$$x_{fd,t_{lam}} = 0.05RePrD \tag{2.8}$$

$$x_{fd,t_{turb}} = 10D \tag{2.9}$$

being $x_{fd,t_{lam}}$ valid for laminar flow, $Re \leq 2300$, and $x_{fd,t_{turb}}$ valid for turbulent flow, $Re > 2300$. In this case the length to achieve fully developed regime is dependent of the Prandtl number.

$$Pr = \frac{\mu Cp}{k} = \frac{\nu}{\alpha} \tag{2.10}$$

where μ is the dynamic viscosity, Cp is the specific heat of the fluid and k is the thermal conductivity of the fluid. This dimensionless number represents the ratio between the momentum diffusivity (kinematic viscosity, ν) and the thermal diffusivity, α. So, it allows to understand the relation between the hydrodynamic and the thermal boundary layers. If $Pr > 1$, the momentum diffusion rate exceeds the energy diffusion rate and the hydrodynamic boundary layer develops more quickly than the thermal one. The opposite occurs for $Pr < 1$ and if $Pr \approx 1$ both boundary layers are comparable. As can be seen in the figure 2.2 the shape of the fully developed temperature profile differs depending on the boundary condition that is imposed on the surface. In thermal boundary layer the temperature profile is continuously changing with the x direction but the shape of this profile, in the fully developed region, no longer changes. So, the condition that needs to be satisfied is:

$$\frac{\partial}{\partial x}\left[\frac{T_s(x) - T(r,x)}{T_s(x) - \overline{T}(x)}\right]_{fd,t} = 0 \tag{2.11}$$

where $\overline{T}$ is the mean temperature of the fluid.

Knowing the two rate equations for heat transferred by conduction (Fourier's law) and by convection (Newton's law of cooling), given by:

Fourier's law:

$$q_s'' = -k\left(\frac{\partial T}{\partial r}\right)_{r=R} \tag{2.12}$$

Newton's law of cooling:

$$q_s'' = h(T_s - \overline{T}) \tag{2.13}$$

where k is the thermal conductivity (W/m·K) ; h is the convection heat transfer coefficient (W/m^2·K); $\overline{T}$ the mean temperature of the fluid and q_s'' the heat flux in the tube wall (W/m^2). Evaluating the equation

2.11 in the tube wall ($r = R$) and applying both laws it can be concluded that in the thermally fully developed flow of a fluid with constant properties, the local convective heat coefficient is a constant independent of the axial position.

So, the equation 2.11 is not valid for the entrance region, as intended. In this region h depends on x, having a large value for $x = 0$, but quickly decreasing, as the thermal boundary layer develops, until it reaches the final value for the fully developed region.

An energy balance to a control volume for the internal flow in the tube is given by:

$$q = \dot{m}Cp(\overline{T_o} - \overline{T_i}) \tag{2.14}$$

where $\overline{T_i}$ and $\overline{T_o}$ are the inlet and outlet mean temperature, respectively. For a constant surface heat flux, since $q = q''_s A$ and knowing that for the round tube $A = \pi DL$. It is easy to obtain the following expression:

$$\overline{T}(x) = \overline{T_i} + \frac{q''_s \pi D}{\dot{m}Cp} x \tag{2.15}$$

From equation 2.15 one can determine how the mean temperature varies linearly with the axial position of the tube.

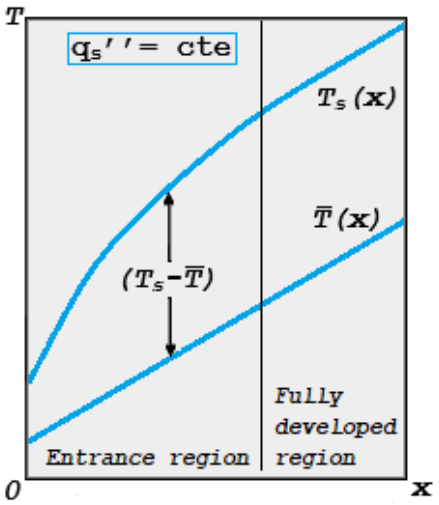

Figure 2.3: Axial temperature variation for a constant surface heat flux applied in a circular tube (adapted from [30]).

For the case considered in this study, a constant heat flux applied in the surface of the tube, $q''_s = constant$, the mean temperatures varies linearly with x. Knowing this and the Newton's law of cooling, presented previously, for the entry region, as h decreases the difference $(T_s - \overline{T})$ will increase with the axial position. Being this difference smaller initially due to the large value of h. For the fully developed region, knowing that h is independent of x, implies that the temperature difference is also independent from x.

Heat transfer

The Grashof number is determined by the following equation:

$$Gr = \frac{g\beta(\overline{T}_s - \overline{T})D^3}{\nu^2} \tag{2.16}$$

where $g = 9.81 m^2/s$ is the gravitational acceleration, $\overline{T}_s$ is the mean surface temperature of the tube, $\overline{T}$ is the mean temperature of the fluid and ν is the kinematic viscosity of the fluid. So, an increase in Grashof number represents an increase of free convection effects, as explained before, when introducing the Richardson number (2.2). Meyer and Everts [41] studied the effects of free convection on the development of the local heat transfer in smooth horizontal circular tubes with an imposed heat flux. They concluded that the transition occurred faster with the increasing Reynolds number due to the increased fluid velocity, i.e, when increasing the Reynolds number above the critical one, the axial

position at which the Nusselt number becomes constant decreases and the value of the Nusselt number increases due to fluid velocity. Although the flow was also influenced by the free convection effects.

So, when free convection effects become significant, at lower Grashof numbers, they disturbed the fluctuations inside the tube, causing a slower transition (axial position) when compared to forced convection conditions, having a dampening effect. As these fluctuations become higher with the Grashof number increases, which leads to enhanced mixing, causing the transition to occur at lower Reynolds numbers, which in turn leads to an increase in the Nusselt number.

The Nusselt number is the most used parameter for studying the heat transfer in an internal flow. This is a dimensionless number that represents the ratio between convection and conduction heat transfer.

$$Nu = \frac{hD}{k} \tag{2.17}$$

All over the years many correlations have been proposed to predict the Nusselt number. Meyer et al. [42], in 2019, performed heat transfer and pressure drop experiments in quasi-turbulent and turbulent flow regimes. Their objective was to combine the laminar and transition correlations with the heat transfer correlations, combining those reported in the literature, to obtain a single and unifying correlation valid for all flow regimes. The correlations they used are presented in the following table.

Correlation	**Eq.**	**Range**
Laminar:		
$Nu = 4.36 + Nu_1 + Nu_2$	(A)	$48 \leq Re \leq 3217$
$Nu_1 = \frac{1}{L}(-0.84Pr^{-0.2}Lt + 0.72(ReD)^{0.54}Pr^{0.34}L_t^{0.46}$		
$Nu_2 = \frac{1}{L}(0.207Gr^{0.305} - 1.19)Pr^{0.42}(ReD)^{-0.08}(L - L_t)$		
$L_t = \frac{2.4RePr^{0.6}D}{Gr^{0.57}}$ for $L > L_t$		
$L_t = L$ for $L < L_t$		
Transition:		
$Nu = (0.017Re - 30.3)Pr^{0.33}Gr^{-0.08}$	(B)	$2115 \leq Re \leq 3586$
Quasi-turbulent and turbulent:		
$Nu = 0.058(Re - 500)^{1.07}Pr^{0.42}(\frac{Pr}{Pr_s})^{0.11}f$	(C)	$2445 \leq Re \leq 401600$
$Nu = 0.018Re^{-0.25}(Re - 500)^{1.07}Pr^{0.42}(\frac{Pr}{Pr_s})^{0.11}$	(D)	
All flow regimes:		
$Nu = [A^{10} + (B^{-8} + C^{-8})^{-10/8})^{0.1}]$	(E)	

Table 2.1: Summary of correlations.

The laminar equation A was developed by Meyer and Everts [41] and is valid for developing and fully developed flow in forced and mixed convection. For quasi turbulent flow, equation C is a function of the friction factor, while equation D has incorporated the Blasius friction factor for smooth tubes. Both equations can be implemented in equation E, however, Meyer et al. [42] suggested the used of the second one, i.e. of equation D, due to its better accuracy. For the transition regime equation B was developed to be implemented in E.

Although the boundaries between laminar and transition flow regimes have been described in literature, they are, in general, depending on visual inspection, for instance looking at the discontinuity observed in the friction factor. This method is subjective and not very accurate. To overcome this issue, Everts and Meyer [43] evaluated the heat transfer in the transition flow regime for developing and fully developed flow in smooth horizontal tubes. To achieve this, a mathematical formulation was used to define the flow regime boundary layers. Nusselt number and Colburn j-factor as a function of Reynolds number were used for that purpose. The Colburn j- factor is given by the equation bellow and represents a dimensionless factor for heat transfer.

$$j = \frac{Nu}{RePr^{1/3}} \tag{2.18}$$

So, the start of the transition flow regime, $Re = Re_{crt}$, was defined as:

$$\frac{dj}{dRe} = 0 \tag{2.19}$$

i.e., the transition starts when the Colburn j-factor gradient changed from negative to positive.

2.2 Nanofluids

Nanofluid is the name given by Choi and Eastman [44], in 1995, to a fluid containing suspended nano-sized particles. This new kind of thermal-fluid has superior thermal properties, as the suspended particles enhance the heat transfer characteristics of the base fluid. In the past few years, a large number of studies have been carried out to investigate nanofluids. Many of them focus on nanofluid development, preparation techniques and characterization, while others are more focused on heat transfer enhancement, convection, applications and challenges [5, 6, 9, 45, 46].

The addition of nanoparticles changes the thermophysical properties of the base fluid, allowing to artificially tune them for a specific application. The most important properties to tune are thermal conductivity, viscosity, density and specific heat.

Since thermal conductivity of the particles is higher than that of the base fluid, an enhancement of the thermal conductivity of the nanofluid is expected to occur. This enhancement depends on some factors related with particle motion, such as the dispersion of the particles, thermophoresis and diffusiophoresis. One of them is the Brownian motion which is the chaotic movement of the ultrafine particles in the base fluid. This motion accelerates the energy exchange and increases with the temperature raise [47]. Other factors influencing the thermophysical properties of the nanofluid, mostly thermal conductivity and viscosity, are the volume concentration, the shape of the particles, the size of the particles, temperature and pH [48, 49].

Effect of concentration

The ultrafine particles with dimensions in the order of 1-100 nm usually do not exceed the 10% volume concentration [9]. This is because the increase in particles concentration represents a raise in thermal

conductivity, but also, an increase in viscosity and a decrease in the stability. Therefore, the goal is to achieve the best thermal properties of the nanofluid with the least possible volume fraction in the base fluid establishing an optimum concentration, according to efficiency and also cost [5, 48].

Although viscosity increases with concentration, some results show that, for volume concentrations lower than 4%, this parameter is not affected [50].

Researches observed that, mainly, the thermal conductivity increased linearly with the increase of particle concentration. However, in some studies, [51, 52], this increase is nonlinear with the volume fraction of the particles.

For the case of specific heat, it is known that, in general, solids present lower values of this parameter than liquids. So, the addition of particles in the base fluid result in a decrease in specific heat capacity of the nanofluid. Since the specific heat is the heat required to raise 1 g of substance by 1^{o}C of temperature, it is desirable the highest value of this parameter, to remove as much heat as possible.

Effect of particle size and shape

Thermal conductivity increases, as well as the viscosity, with the decrease in particles size, due to an enlarged surface to volume ratio. This is the result of numerous investigations, however, in a few studies, such as that reported by Beck et al. [53], the results show a decrease of thermal conductivity enhancement with the decrease of the particle size. On the other hand, when the shape of the nanoparticles is deviated from the spherical one, the thermal conductivity increases. So, cylindrical particles have higher thermal conductivity, due to a higher aspect ratio, that allows faster heat transport. However, this type of particles increase the viscosity of the fluid.

Effect of temperature

The majority of studies evaluating the influence of temperature demonstrate that as the temperature increases, the thermal conductivity of the nanofluids also increases. However, in a few studies, [54], the results show an inverse relation of this factors. For the case of viscosity, the general results show a decrease with temperature increment.

Effect of pH

The pH of the nanofluid affects simultaneously the thermal conductivity and the viscosity, as well as the stability of the nanofluid. Given this, there is a specific value for the pH that results in the highest thermal conductivity and the lowest viscosity. However, due to the pH related problems, such as damages that can be caused in the heat transfer surfaces, it is, in general, recommended to keep pH value neutral.

2.2.1 Consequences for the fluid dynamics and heat transfer characteristics in internal flows

The variations of the previously explained thermophysical properties of the nanofluids are the factors that influence the hydrothermal characteristics of the nanofluid. The most important parameters to analyze are the heat transfer coefficient, Nusselt number, Prandtl number as well as the pressure losses. Given this, the thermal conductivity will affect directly the Nusselt and Prandtl numbers, fundamental parameters to analyze the heat capacity of the fluid.

The other important parameter to be analyzed before apply the fluid to a practical case is the the flow resistance, i.e the pressure drop, which is directly affected by the viscosity of the nanofluid. The increase of the viscosity represents an increase of the pressure drop, which is not desirable, as it means an increase in the pumping power. On the other hand, viscosity directly affects the convective heat transfer coefficient.

Since thermal conductivity has been expressed to be the most important parameter responsible for the enhancement of heat transfer, many studies have been published on this aspect. Alumina and copper oxide, Al_2O_3 are the most common nanoparticles used by researchers. All the experiments carried out with this type of nanoparticles resulted on a thermal conductivity enhancement with the increase in nanoparticles concentration [55].

However, a thermal conductivity enhancement of 100% was reported with aqueous-based MWCNT (multi walled carbon nanotubes) nanofluids at 2.5% in volume of nanotubes. Higher increases were obtained using magnetic nanoparticles dispersed under an applied magnetic field, which reduces its applicability in industry [48].

Also, many research has been published for experimental heat transfer characteristics of various types of nanofluids. For forced convection in smooth, horizontal tubes with a constant heat flux applied, Pak and Cho [56], in 1998, studied the turbulent friction and heat transfer of $Al_2O_3/water$ and $TiO_2/water$ nanofluid. Their results showed that heat transfer increased with increasing volume concentration, for 1.34% volume of Al_2O_3 particles the enhancement was 45% and 75% at a concentration of 2.78%. At the same concentration the heat transfer enhancement for $TiO_2/water$ was less than that of $Al_2O_3/water$. However, under the condition of constant average velocity, for 3% volume concentration, the heat transfer coefficient was 12% smaller than that of the base fluid.

Li and Xuan [8, 57] studied, in 2002 and 2003, the laminar and turbulent convective heat transfer and friction factor of $Cu/water$ nanofluid. The suspended particles enhance the heat transfer process, increasing the heat transfer coefficient about 60% for 2.0% volume concentration of Cu nanoparticles.

Maïga et al. [58], in 2005, studied the laminar forced convection flow of $Al_2O_3/water$ and Al_2O_3/ ethylene glycol. They observed that the increase in nanoparticles concentration clearly increased the heat transfer coefficient and this enhancement also increases with the augmentation of the Reynolds number. However, the mixture with ethylene glycol offered better heat transfer properties than the one with water. one year later, Maïga et al. [59] studied the hydrodynamic and thermal behavior of $Al_2O_3/water$ in the turbulent flow. As well, they concluded that the inclusion of the nanoparticles in the base fluid

produced an increase of the heat transfer coefficient and this effect was more pronounced for flows with high Reynolds number.

In 2009, Anoop et al. [60], used Al_2O_3 particles dispersed in water to evaluate the effect of particle size on convective heat transfer in laminar developing region. With the increase in particle concentration and flow rate, the average heat transfer coefficient value was increased. However, for the nanofluid with 45 nm particles, the enhancement was around 25%, while for the nanofluid with the 150 nm particles, at the same conditions, the enhancement was only 11%.

The forced convection heat transfer in the fully developed turbulent regime was also investigated by Vajjha et al. [61] in 2010. They tested Al_2O_3, Cu and SiO_4 dispersed in 60% ethylene glycol and 40% water. The results showed a linear relation between the particle concentration and heat transfer, fluid density, viscosity and pressure drop. The highest value of heat transfer and pressure drop was obtain by Al_2O_3 particles, followed by Cu and SiO_4.

The effects of $Al_2O_3 - Cu$ nanoparticles in water, an hybrid nanofluid, were investigated by Suresh et al. [62] in 2012. In this study, fully developed, laminar convective heat transfer for 0.1% volume concentration were evaluated in an uniformly heated circular tube. Their results show an average increase in Nusselt number of 10.94%, being the maximum enhancement of 13.56% for a Reynolds number of 1730, when compared to water. When compared to $Al_2O_3/water$ nanofluid, the hybrid nanofluid has higher friction factor, causing extra penalty in pumping power. In 2015, Moghadassi et al. [63] realized a numerical study of water based Al_2O_3 and $Al_2O_3 - Cu$ hybrid nanofluid, for the same conditions that [62]. The results revealed that adding a small amount of Cu particles increase the heat transfer by about 5%.

As aforementioned, Meyer et al. [34], in 2013, also investigated nanofluids. Particularly, they studied the convective heat transfer coefficient of aqueous suspensions of multi walled carbon nanotubes in the laminar, transition and early turbulent flow regimes, with a constant heat flux. When comparing the data on a Reynolds-Nusselt graph, the heat transfer was enhanced. However, the nanofluids showed a decrease in heat transfer coefficient, in relation to distilled water, when compared at the same velocity. This is due to the fact of the $MWCNT/water$ nanofluids have larger viscosity than water. It also led to an increase of the pressure drop with the increasing volume concentration.

The literature review introduced in the previous paragraphs provide the context for the investigation of the effects of adding nanoparticles on the convective heat transfer in a horizontal, circular, smooth tube with constant heat flux condition. Most of the published data show a thermal conductivity and a heat transfer coefficient enhancement with increased particle concentration, being the heat transfer coefficient enhancement more pronounced for flows with high Reynolds number. However, different results of this coefficient were reported depending from the analysis method. On the other hand, a penalty in pumping power for using the nanofluids is also reported, due to a increase of the friction factor.

2.2.2 Preparation and stabilization of the nanofluid

The preparation of the nanofluid is a key step to obtain a improved fluid. This is because the preparation directly influences the stability of the nanofluid. The factor which makes the nanofluid unstable is the proneness of the particles to aggregate with time due to very strong van der Waals interaction forces. This agglomeration of nanoparticles results in the clogging of the channels, which represents a decrease of the heat transfer area but also a decrease of the thermal conductivity of the nanofluid. Since the thermal conductivity is directly or indirectly reduced with instability, there is a loss of the potential benefits for using the nanofluid if it is not stable.

So, proper mixing and stabilization of suspensions is one of the most important aspects. There are some methods that can be applied to the nanofluid for a long term stability, which can be divided in chemical and physical methods [48, 64].

Chemical methods

The pH control consists in the manipulation of zeta potential far from the isoelectric point (IEP). In this point, zeta potential value is zero, meaning that repulsive forces between nanoparticles suspended in the base fluid are zero causing a tendency for coagulation, turning the nanofluids unstable. However, as explain before, it is better, for safety reasons to keep the pH of the nanofluid neutral. The modification of the nanoparticles surface is also a chemical method used. It consists in the introduction of modified nanoparticles, by functionalization, in the base fluid. This functionalized particles can provide stability to the nanofluid. A third method is the addition of surfactants in the nanofluid. By decreasing the surface tension of the base fluid, the surfactants aid the nanoparticles to uniformly spread throw the base fluid, representing an effective and economic way to enhance stability. Care must be taken however, since in some cases, the surfactant may increase the thermal resistance between the nanoparticles and the base fluid.

Physical methods

Physical methods can be applied to the mixture, for instance, ultrasonication, which consists in applying sound energy for some period of time. This energy will disperse the nanoparticles in the base fluid and break clusters. The optimum sonication conditions, e.g. power and frequency levels, may differ according to the type of particle. type of base fluid, concentration, etc. Ultrasanication baths or probes can be used, being the latter the most common physical method used. Other physical method used is the homogenization, being the high shear homogenizer, as well as the high pressure homogenizer effective tools to obtain stable nanofluids.

Chapter 3

Experimental section

This section describes in detail the experimental setup and instrumentation used, as well as all of the experimental procedures followed to prepare and characterize the nanofluids and to perform the experiments. This section also includes the description of the data reduction and of the uncertainties.

3.1 Experimental setup description

The experimental setup used in this study (represented in Figure 3.1) was the one previously used in Nikulin et al. [65]. Its main description is summarized bellow.

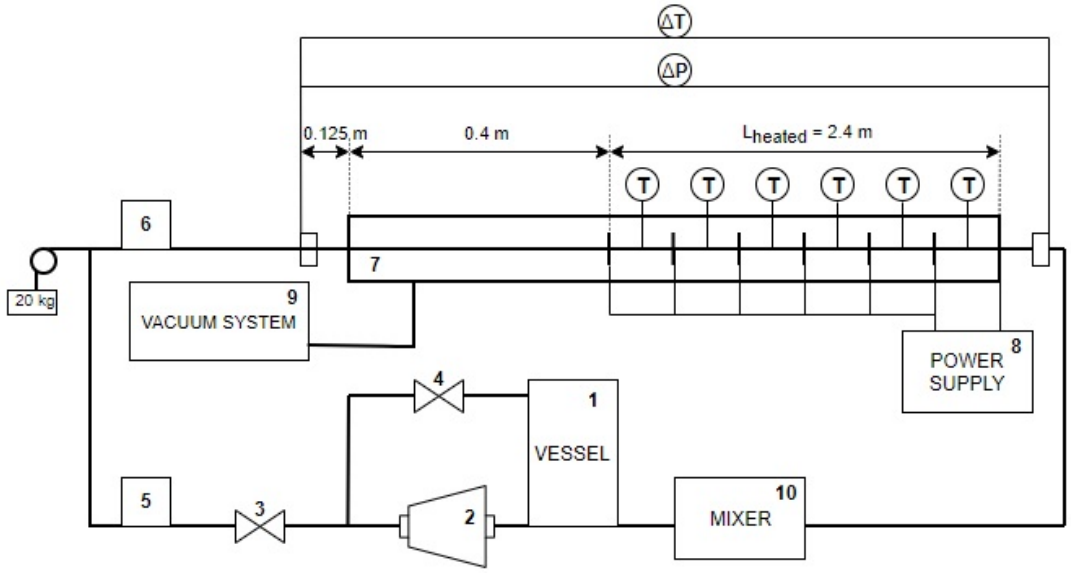

Figure 3.1: Schematic diagram of the experimental setup.

The working fluid is introduced in the vessel (1) and is pumped by a magnetically coupled vane pump (2) through the closed loop. The pump is connected to a frequency converter (5) that allows to regulate the flow rate of the working fluid. The flow rate can also be regulated by a bypass valve (4). Once the valve is open it forces the fluid to recirculate to the vessel, reducing the flow in the installation. After the pump, the fluid enters a Coriolis mass flow meter (mini CORI-FLOW M15, Bronkhorst) (6) where the

mass flow rate, $\dot{m}$, the inlet temperature, T_i, and the density of the fluid, ρ, are measured. Working in the range of 0.2 to 300 kg/h, with an accuracy of 0.2% and with a density accuracy of 5 kg/m^3. Then, it goes through the test section (7), a smooth round tube with 3.5 mm in inner diameter and 0.25 mm in wall thickness. A initial 0.4 m of length without heating is used for flow developing. The heated area has 2.4 m and is divided into six equal parts with six type K thermocouples (T) installed on the tube wall. A constant heat flux is applied to the walls of this section by a power source (HY5050EX, VOLTEQ)) (8), which allows to regulate the electrical current, I, with an accuracy of 0.5% and the voltage, V, with an accuracy of 0.3% . Also, two thermocouples are placed at the entry and outlet of the test section, which provide the temperature variation in the tube (ΔT). A differential pressure transducer (PX2300, Omega) (ΔP) provides the pressure difference along the test section. To prevent heat loss the test section is inside a vacuum chamber (9) and all the pipes in the setup are insulated by a rubber insulation. Finally, the fluid enters the mixer, cooler and heating system (10), before returns to the vessel and close the loop. To make sure that the test section is in the horizontal and straight position a stretching force of 20 kg is used.

All the pressure and temperature signals from the sensors are acquired by a RIGOL acquisition system, connected to a PC with its own software. The data from the Coriolis mass flow meter is processed by the software FlowDDE.

3.2 Experimental procedure

The experimental process consisted in testing four fluids at three different inlet temperatures. The fluids tested were pure tetralin and C_{60}/tetralin nanofluid with 0.10%, 0.30% and 0.66 mass% of nanoparticles. The temperatures at which they were tested were 25º, 35º and 45ºC.

For all the tests carried in the experimental setup it has been followed the next procedure:

1. Turn on the RIGOL acquisition system and its software;
2. Turn on the frequency converter and the FlowDD software;
3. Turn on the hydraulic pump through the frequency converter;
4. Turn on the mixture system;
5. Turn on the vacuum chamber;
6. Verify if the temperature of the fluid is the one desired $\pm$ 1ºC,
   (a) If the temperature is lower than the desirable one, connect the heating system until reach it;
   (b) If the temperature is higher than the desirable one, connect the cooling system until reach it.
7. Adjust the frequency converter or the valve (main use of the converter) to achieve the mass flow rate required.
8. Wait until the pressure and temperature sensors show stabilized values.

9. Save the data;

10. Turn on the power source;

11. Wait until the sensors of pressure and temperature show stabilized values.

12. Save the data;

13. Turn off the power source;

14. Return to point 6.

The next two tables present the ranges, for each temperature measured, of measured and calculated parameters characterizing the working conditions for the four fluids. In table 3.1 the tabled values are from the experimental tests carried out with heat flux applied to the test section. While, in the case of table 3.2, the values are from the experimental tests with no heat flux applied to the test section.

Parameters	**25ºC**	**35ºC**	**45ºC**	**Units**
Mass flow rate, $\dot{m}$	0.00212 - 0.02538	0.00177 - 0.02252	0.00149 - 0.01953	[kg/s]
Inlet temperature, T_i	23.56 - 26.08	34.12 - 36.86	42.92 - 46.30	[ºC]
Heat flux, q''_{imp}	4.5 - 10.6	4.4 - 10.4	4.4 - 10.3	[kW/m^2]
Mean surface temperature, $\overline{T_s}$	29.63 - 52.39	39.65 - 64.75	49.95 - 87.84	[ºC]
Mean fluid temperature, $\overline{T}$	26.70 - 39.41	36.98 - 51.74	47.55 - 69.81	[ºC]
Temperature difference, ΔT	4.38 - 27.51	5.01 - 31.88	5.54 - 49.12	[ºC]
Reynolds number, Re	494 - 5721	576 - 6189	524 - 6724	[-]
Prandtl number, Pr	17.07 - 23.57	13.63 - 21.33	10.32 - 19.89	[-]
Nusselt number, Nu	7.65 - 73.44	7.35 - 84.71	7.32 - 98.03	[-]
Grashof number, Gr	230.54 - 2223.11	292.74 - 3729.81	438.87 - 439.69	[-]
Richardson number, Ri	0.00001 - 0.0064	0.00001 - 0.00935	0.0002 - 0.01801	[-]
Colburn j-factor, j	0.00136 - 0.00558	0.00139 - 0.00564	0.00155 - 0.00633	[-]

Table 3.1: Ranges of parameters with heat flux applied to the test section.

Parameters	**25ºC**	**35ºC**	**45ºC**	**Units**
Mass flow rate, $\dot{m}$	0.00207 - 0.02576	0.00171 - 0.02250	0.00146 - 0.01951	[kg/s]
Inlet temperature, T_i	23.44 - 26.22	33.78 - 36.22	43.06 - 46.82	[ºC]
Mean fluid temperature, $\overline{T}$	23.54 - 26.23	33.77 - 35.93	42.55 - 46.24	[ºC]
Mean surface temperature, $\overline{T_s}$	23.66 - 26.15	33.35 - 35.67	42.06 - 45.49	[ºC]
Pressure drop, ΔP	3447 - 115386	2434 - 88637	1321 - 67474	[Pa]
Friction factor, f	0.0331 - 0.18208	0.03252 - 0.17120	0.03151 - 0.16099	[-]
Reynolds number, Re	398 - 5586	427 - 5804	443 - 6254	[-]

Table 3.2: Ranges of parameters with no heat flux applied to the test section.

3.3 Preparation and characterization of the nanofluids

In this study, particles of fullerene, C_{60} (CAS 99685-96-8) with a purity of 98%, were used to prepare the nanofluid. Before the experimental procedure took place, it was necessary to evaluate the stability and solubility of the C_{60} nanoparticles in the base fluid.

First, two samples were tested with 1 mass% of nanoparticles, one with oil and tetralin as base fluid and the other one with just tetralin as the base fluid. Since the particles did not dissolve as desirable in the first sample, tetralin was selected as the working fluid. A sample of tetralin (1,2,3,4-Tetrahydronaphthalene, CAS 119-64-2) is shown in figure 3.2.

Figure 3.2: Sample of Tetralin.

Once the working base fluid was chosen, three different concentrations of particles were tested. Samples were prepared diluting the nanoparticles in the base fluid and using sonication to homogenize and minimize the chances of particle agglomeration. Samples with 0.10%, 0.30% and 0.66 mass% of nanoparticles are shown in figure 3.3. From a visual inspection to the samples depicted in the figure it is possible to state that the nanofluids are stable and homogeneous, with no sedimentation.

(a) 0.10 mass% (b) 0.30 mass% (c) 0.66 mass%

Figure 3.3: Samples of nanofluid.

The mass fraction of the nanoparticles in the samples was determined by the following equation:

$$w = \frac{m_{np}}{m_{np} + m_{bf}} \tag{3.1}$$

where m_{np} is the mass of nanoparticles (kg) and m_{bf} is the mass of tetralin (kg). The mass measurements where made in an analytical balance (model ABS80-4N by Kern) with a resolution of 0.1 mg and an accuracy of 0.3 mg (figure 3.4(a)).

The total mass of tetralin used for the tests in the experimental setup was 1447.448 gr. Table 3.3 presents the exact mass of C_{60} used for each concentration.

Nanofluid	Mass C_{60} (gr)	Mass fraction (%)
a	1.5005	0.10356
b	4.3485	0.29953
c	9.5475	0.65529

Table 3.3: Nanofluid concentrations.

Ultrasonication was used to break the nanoparticles cluster and form a well dispersed suspension. The power applied was fixed for the three concentrations, to the value of 35 W. An amplitude of 50% and a pulse of 80% were applied during a period of 50 minutes for the nanofluid a, and, during a period of 120 minutes for the nanofluid b. For the nanofluid c, with the highest concentration, was firstly sonicated for 3 hours and 30 minutes using an amplitude of 30% and a pulse of 70%. This solution was then sonicated for 60 minutes using an amplitude of 90% and a pulse of 80%. Figure 3.4 illustrates the equipment used to prepare nanofluids, namely the precision balance (a) and the sonicator (b) (model UP200Ht by hielscher).

(a) Analytical balance

(b) Sonicator

Figure 3.4: Instrumentation.

3.3.1 Thermophysical properties

To characterize the hydrodynamic and thermal properties of the flows under the tested conditions, it is important to evaluate the thermophysical properties of tetralin and C_{60}/tetralin nanofluid. Density, viscosity, thermal conductivity and specific heat capacity were obtained using the methods described in the following paragraphs.

Density

The density of the nanofluid, ρ_{nf}, is in general considered to be a mixed property of the density of base fluid, ρ_{bf}, and the density of nanoparticles, ρ_{np}. So, a widely used equation for this calculation is:

$$\rho_{nf} = \phi\rho_{np} + (1-\phi)\rho_{bf} \tag{3.2}$$

where ϕ is the particle volume fraction obtained by equation 3.3, where, respectively, w is the mass fraction of the nanoparticles, obtained by equation 3.1.

$$\phi = \frac{\frac{w}{\rho_{np}}}{\frac{w}{\rho_{np}} + \frac{1-w}{\rho_{bf}}} \tag{3.3}$$

Gonçalves et al. [66] reported some measurements of density and viscosity of tetralin. Their results where compared to the density obtained by the Coriolis mass flow meter in the present study.

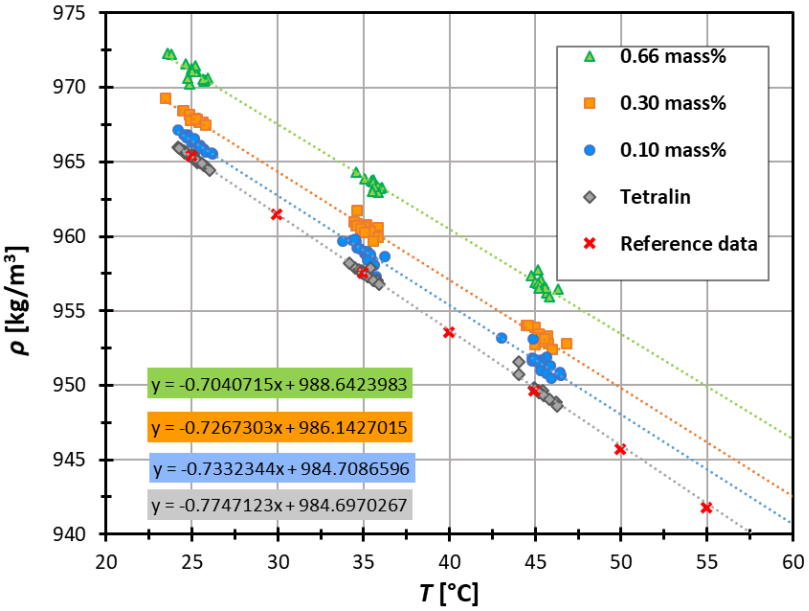

Figure 3.5: Density versus temperature as a function of nanoparticles mass fraction.

It is clear from figure 3.5 that the values of density increase with the mass fraction of the particles and decrease as the temperature increase, as expected, according to the open literature. The results obtained for tetralin clearly match with those reported in the reference data [66]. So, the equations presented in the graphic were used for density calculation in function of the temperature and also mass concentration of the nanofluid.

Viscosity

To obtain the dynamic viscosity a previous analysis to the fluid had to be performed. The dependence of shear stress (τ) versus shear rate ($\dot{\gamma}$) was calculated using the next two equations, respectively:

$$\tau = \frac{D}{4L}\Delta P \tag{3.4}$$

$$\dot{\gamma} = \frac{32}{\pi D^3} Q \tag{3.5}$$

Equations 3.4 and 3.5 were both used in laminar flow with no heat flux applied. The results, figure 3.6, show that C_{60}/tetralin nanofluid is a Newtonian liquid, regardless of the concentration or temperature, and, given this, by implementation of capillary rheometer theory, the equation of viscosity of Hagen-Poiseuille is applicable:

$$\mu = C \frac{\Delta P}{Q} \tag{3.6}$$

where C is a constant related to the dimensions of the tube and Q is the volumetric flow rate (m^3/s). The results, shown in figure 3.7, follow the reference data 2.2, so, as expected the dynamic viscosity of all fluids tested, clearly increases with mass concentration of the nanofluids and decreases with temperature raise.

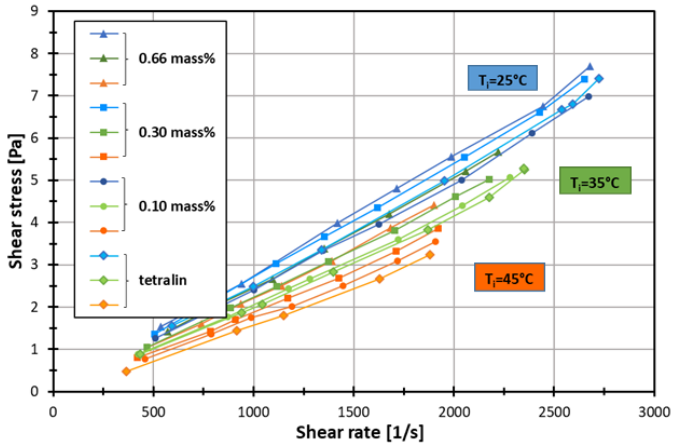

Figure 3.6: Shear stress versus shear rate as a function of temperature and nanoparticles mass fraction.

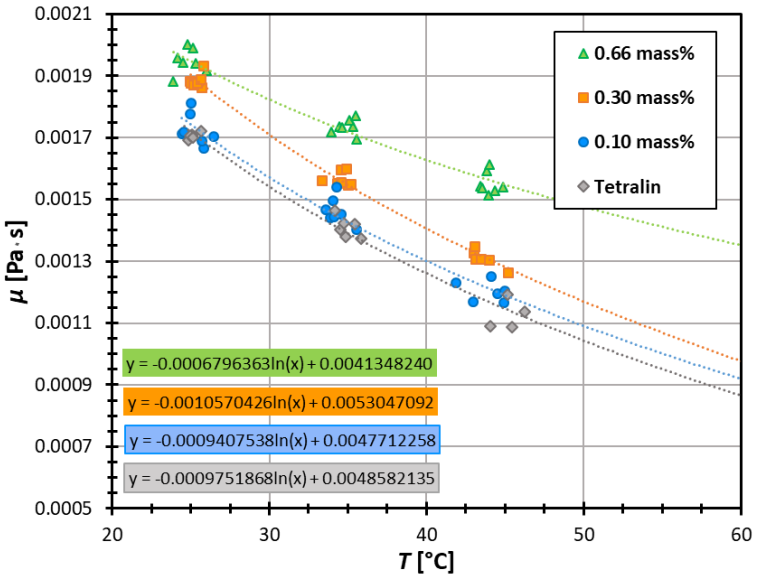

Figure 3.7: Dynamic viscosity versus temperature as a function of nanoparticles mass fraction.

Thermal conductivity

The thermal conductivity of tetralin and C_{60}/tetralin nanofluids was measured by the transient hot wire method. There are several techniques used for this purpose, however, the transient hot wire technique is the most adequate due its accuracy, as it eliminates the errors caused by natural convection in the nanofluid, and it is very fast compared to other techniques [48, 54]. This method consists in immersing a wire in the sample fluid in which thermal conductivity is to be measured. A tantalum wire with a diameter of 25 μm divided into two sections with different lengths was used in this measurement. The use of two sections with different lengths allows to eliminate the systematic uncertainty associated with edge heat losses. This wire serves as heat source, the heat generated increases the temperature of the wire and of the sample fluid. This increase of the wire temperature depends of the thermal conductivity of the fluid, functioning the wire, as well, as a temperature sensor. The ideal mathematical model of the method is based on Fourier's law, assuming the hot wire as an ideal, infinite thin and long heat source in an infinite surrounding with constant initial temperature. The results were obtained with an experimental cell, especially created to implement this method, and following the recommendations of Antoniadis et al. [67].

The results were obtained with an uncertainty of 3%, and were compared those reported by Vargaftik [68] obtaining a maximum deviation of 1.86% for tetralin.

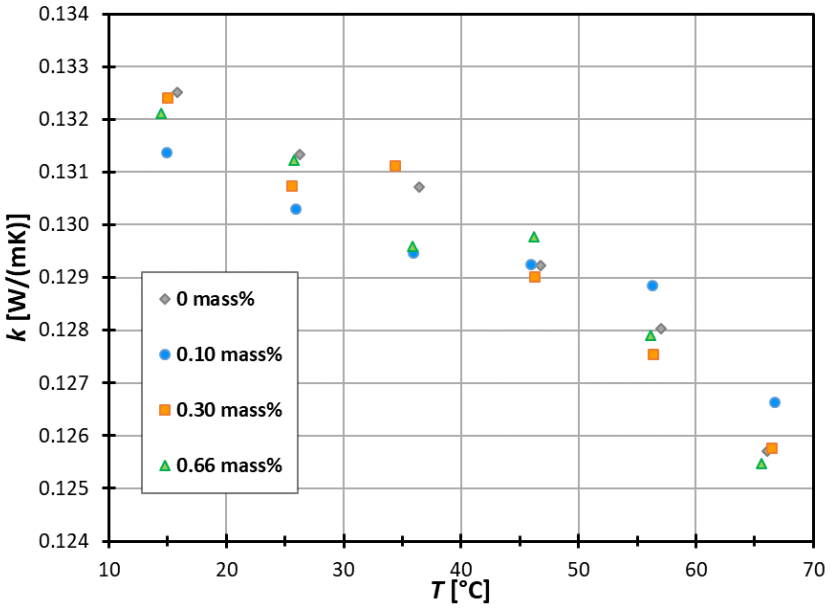

Figure 3.8: Thermal conductivity versus temperature as a function of nanoparticles mass fraction.

As explained before, in 2.2, in the majority of the studies reported in the literature, the results show a general increase in thermal conductivity with both, temperature and nanoparticles concentration augmentation. However, since the thermal conductivity of liquid tetralin decreases as the temperature increases, as can be seen in Vargaftik [68], the thermal conductivity of C_{60}/tetralin nanofluid has to decrease, figure 3.8.

On the other hand, there is no clear relation between the thermal conductivity and the nanoparticles

mass fraction. Since there is no measurement data to compare it, it is difficult to know what to expect. However, since the uncertainty of the experimental data on thermal conductivity was estimated at 3%, and that the maximum deviation between the experimental results is 1.25%, it is possible to conclude that the effects of the mass concentration in the thermal conductivity are negligible, due to the low sensitivity of the measurements procedure. Also, in a study published by Tawfik [69] on nanofluids thermal conductivity enhancement, Tawfik [69] concluded that fullerenes showed lower enhancement of thermal conductivity when compared to other particles. As an example, for 0.378 volume% concentration the enhancement was around 0.816%.

Specific heat capacity

The specific heat used in this thesis was obtained by Zhelezny et al. [70, 71], being the equation used for Cp calculation the following:

$$Cp = a + b \cdot T^3 \tag{3.7}$$

where a and b are two coefficients dependent on the nanofluid mass concentration (the values used for these constants are summarized in the next table) and T is the temperature in Kelvin.

	a	b
0 mass%	1284.496	$1.30334 \cdot 10^{-5}$
0.10 mass%	1279.794	$1.31386 \cdot 10^{-5}$
0.30 mass%	1270.390	$1.33490 \cdot 10^{-5}$
0.66 mass%	1237.476	$1.37698 \cdot 10^{-5}$

Table 3.4: Coefficient values for equation 3.7.

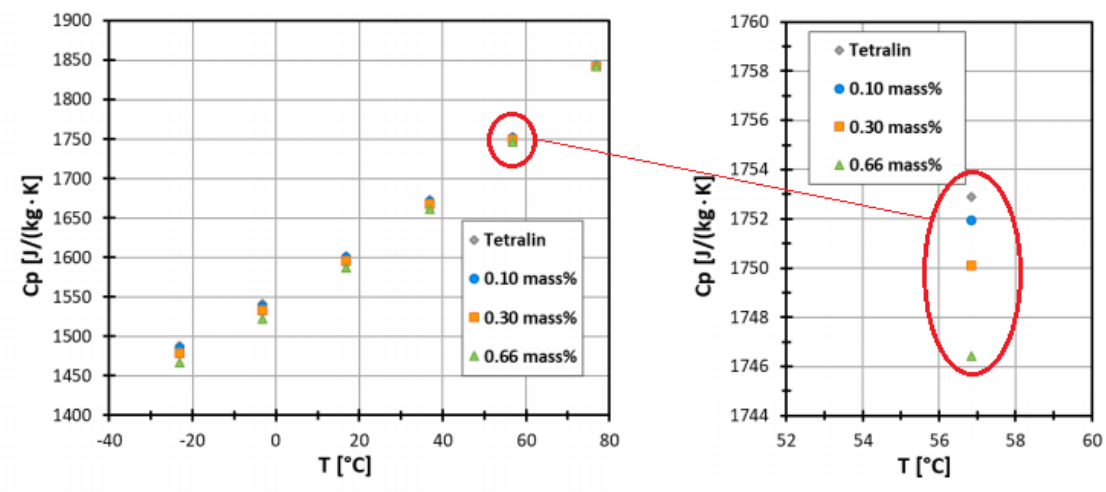

Figure 3.9: Specific heat capacity versus temperature as a function of nanoparticles mass fraction.

In figure 3.9 it is represented the specific heat capacity as a function of temperature and nanoparticles mass fraction. The results show an increase of this value with temperature raise, as well as a small

decrease with nanoparticles mass fraction raise, being this difference, with respect to tetralin, smaller as the temperature raises, as can be seen in the figure detail.

3.4 Data reduction

The thermophysical properties of the four tested fluids, i.e. density ρ, dynamic viscosity μ, thermal conductivity k and specific heat capacity C_p, were evaluated at the mean temperature of the fluid ($\overline{T}$):

$$\overline{T} = Ti - \frac{\Delta T}{2} \tag{3.8}$$

where ΔT is the temperature difference between the outlet and inlet temperatures of the tube, $\Delta T = T_o - T_i$.

The Reynolds number were calculated with:

$$Re = \frac{4\dot{m}}{\mu\pi D} \tag{3.9}$$

The friction factor was calculated using the Darcy-Weishbach equation:

$$f = \frac{2D\Delta P}{\rho U^2 L} \tag{3.10}$$

where U is the mean velocity of the flow, and is calculated by:

$$U = \frac{\dot{m}}{\rho A_c} \tag{3.11}$$

where $A_c = 9.6486$ mm^2 is the cross section area of the tube ($A_c = \pi D^2/4$).

The thermal power transferred to the fluid is given by:

$$q = \dot{m}Cp\Delta T \tag{3.12}$$

which divided by the surface area of the heated length of the tube, $A = 0.026427$ m, ($A = \pi D L_{heated}$) allows to calculate the heat flux, $q'' = q/A$. The heat transfer coefficient is then given by:

$$h = \frac{q}{(\overline{T_s} - \overline{T})} \tag{3.13}$$

where $\overline{T_s}$ is the surface mean temperature and is calculated by an average of the temperature values of each six thermocouples installed on the tube wall.

$$\overline{T_s} = \frac{T_1 + T_2 + T_3 + T_4 + T_5 + T_6}{6} \tag{3.14}$$

Then, a number of dimensionless numbers are calculated, which are relevant to analyze the flows of

the nanofluids, namely, the Nusselt number;

$$Nu = \frac{hD}{k} \tag{3.15}$$

Prandtl number:

$$Pr = \frac{\mu Cp}{k} \tag{3.16}$$

Grashof number:

$$Gr = \frac{g\beta(\overline{T}_s - \overline{T})D^3}{\nu^2} \tag{3.17}$$

Richardson number:

$$Ri = \frac{Gr}{Re^2} \tag{3.18}$$

Colburn j-factor:

$$j = \frac{Nu}{RePr^{1/3}} \tag{3.19}$$

3.5 Uncertainties

The deviation between a measurement and the true value of a specific quantity to be measured is the measurement error, i.e, the result of a measurement is only an approximation of its real value. So, a measurement is only complete when accompanied by its uncertainty, as explained by Taylor and Kuyatt [72].

According to the *International Committee for Weights and Measures* (CIPM) approach, these uncertainties, which consist on several components, can be grouped into two categories, one evaluated by statistical methods, and other evaluated by other means, being commonly classified as components of uncertainty rising from a random effect or as components of uncertainty rising from systematic effects. The random effect gives rise to a possible random error while the systematic effect gives rise to a systematic error.

The systematic error is the one related to accuracy. It is repetitive and constant and can be reduced or even eliminated by the proper means, such as calibration. This type of errors are, in general, supplied by the producer. On the other hand, the random errors are related to precision. They are inconsistent and non-repetitive and can only be reduced. This type of error can be estimated by the statistical analysis of series of observations.

The combination of both types of uncertainties gives rise to the combined standard uncertainty, whose symbol is u_c. The method to obtain this value is often called the *law of propagation of uncertainty*, and can be calculated as:

$$u_c^2(y) = \sum_{i=1}^{N} \left(\frac{df}{dx_i}\right)^2 u^2(x_i) \tag{3.20}$$

where df/dx_i are the sensitive coefficients, and $u(x_i)$ is the standard uncertainty associated with the input x_i.

The input uncertainties for equation 3.20 are summarized in table 3.5. The main uncertainties determined for the parameters analyzed in the present study are depicted in table 3.6.

Parameters	**Uncertainty**	**Units**
Mass, m	0.3	[mg]
Inner diameter, D	0.05	[mm]
Length of the tube, L	2	[mm]
Inlet temperature, T_i	0.1	[^{o}C]
Mean surface temperature, $\overline{T_s}$	0.1	[^{o}C]
Temperature difference, ΔT	0.1	[^{o}C]
Mass flow rate, $\dot{m}$	0.2	[%]
Electrical current, I	0.5	[%]
Voltage, V	0.3	[%]
Thermal conductivity, k	3	[%]
Specific heat capacity, Cp	1	[%]
Density, ρ	5	[kg/m^3]

Table 3.5: Uncertainty for input parameters to equation 3.20.

Parameters	**Maximum uncertainty**	**Units**
Mass fraction, w	4.398$\cdot 10^{-7}$	[kg/kg]
Pressure drop (range 0-68947.6(Pa)), ΔP	262.8	[Pa]
Pressure drop (range 0-689476(Pa)), ΔP	2628	[Pa]
Dynamic viscosity, μ	0.1637	[mPa$\cdot$ s]
Reynolds Number, Re	1.761	[%]
Friction factor, f	0.00505	[-]
Heat rate imposed to the wall, q_{imp}	1.879	[W]
Heat rate received by the fluid, q_{real}	5.674	[W]
Heat transfer coefficient, h	7.554	[%]
Nusselt number, Nu	9.529	[%]

Table 3.6: Maximum combined global uncertainty.

Chapter 4

Analysis of results

Hydrodynamic and heat transfer characteristics of tetralin and C_{60}/tetralin nanofluid with 0.10%, 0.30% and 0.66 mass% of particles were evaluated in a circular tube at 25º, 35º and 45ºC of inlet temperature, from laminar to turbulent flow regime.

4.1 Experimental setup validation

As explained before in chapter 3, the experimental setup used here was previously used and validated by Nikulin et al. [65]. However, to ensure the validity of the results obtained for the particular conditions considered in this study, an additional validation was performed with water at 25ºC. The obtained experimental data of the friction factor was then compared against theoretical correlations. In the laminar region the correlation used was Hagen-Poiseuille equation, $f = 64/Re$, while in the turbulent region, the Blasius equation was used, $f = 0.316Re^{-1/4}$.

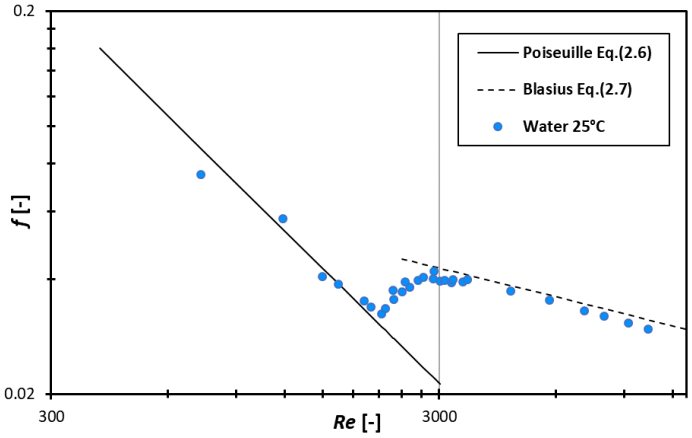

Figure 4.1: Friction factor of water as a function of Reynolds number.

Figure 4.1 clearly shows that the experimental results agree very well with the theoretical correlations. For the laminar region the average deviation was 6.56%, with a maximum deviation of 14.61%. For the turbulent region the average deviation was 4.67%, with a maximum deviation of 7.34%.

4.2 Flow conditions

To assess the flow conditions inside the tube, hydrodynamic and thermal entry lengths were calculated. The hydrodynamic entry length is calculated by equations 2.3 and 2.4. So, as can be noticed in these equations, this length just depends on the tube diameter and on the Reynolds number, not being affected by the type of fluid used. So, the flow will be, for laminar and turbulent regions, hydrodynamically fully developed, regardless of the concentration of the nanofluid being used. This result is demonstrated in figure 4.2.

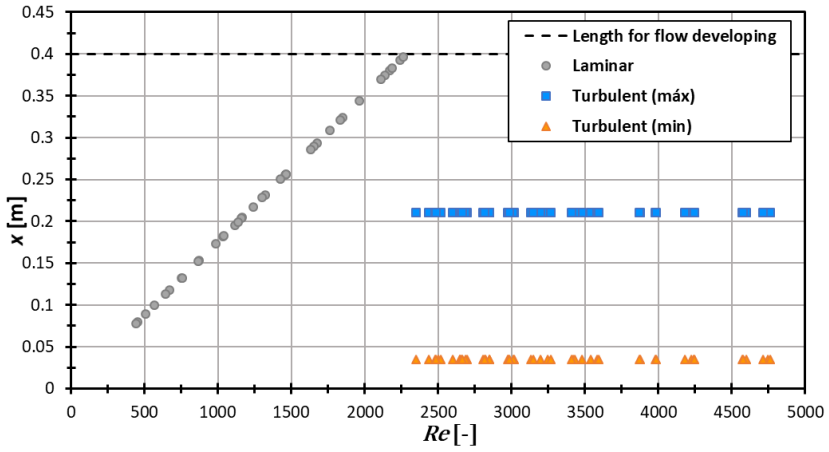

Figure 4.2: Hydrodynamic entry length as a function of Reynolds number.

For turbulent flow, $Re > 2300$, the hydrodynamic entry length obtained was $0.0351 \leq x_{fd,h_{turb}} \leq 0.2103$ m. For the laminar region, $Re \leq 2300$, the maximum value that can be obtained is 0.4029 m for a Reynolds number of 2299. This value is slightly higher than the initial length of the test tube (0.4 m), however, this difference is so small that can be concluded that the test section will always have hydrodynamically fully developed flow, according to the definition explained in section 2.1.1.

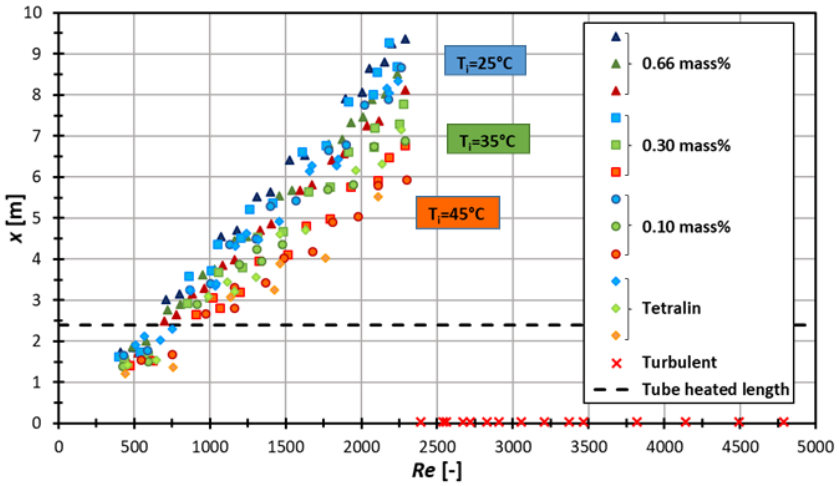

Figure 4.3: Thermal entry length as a function of Reynolds number, temperature and nanoparticles mass fraction.

For the thermal entry length properties of the flow affect this value in the laminar flow regime, as the

thermal entry length in this region depends on the Prandtl number.

However, for all the tests carried in this study, the results are similar, as depicted in figure 4.3. In the laminar region, the flow will be developing thermally, since the test section length is not enough for the flow to develop. For the turbulent region, $Re > 2300$, $x_{fd,t_{turb}} = 0.0351$ m, which is much smaller than the heated length of the test section $L_{heated} = 2.4$ m. So, for this region the flow will be fully developed thermally.

4.3 Convection analysis

The convection type in the flow was identified based on the Richardson number method, as explain in section 2.1. Knowing that the Grashof number depends on the difference between the surface mean temperature and the mean temperature of the fluid, the higher the inlet temperature, the higher tends to be this difference and, so, the higher will be the Richardson number, thus determining a limiting value. Hence, although the four fluids were evaluated at the three inlet temperatures, the results on the Richardson number are only shown here, in figure 4.4, for the highest inlet temperature of 45°C.

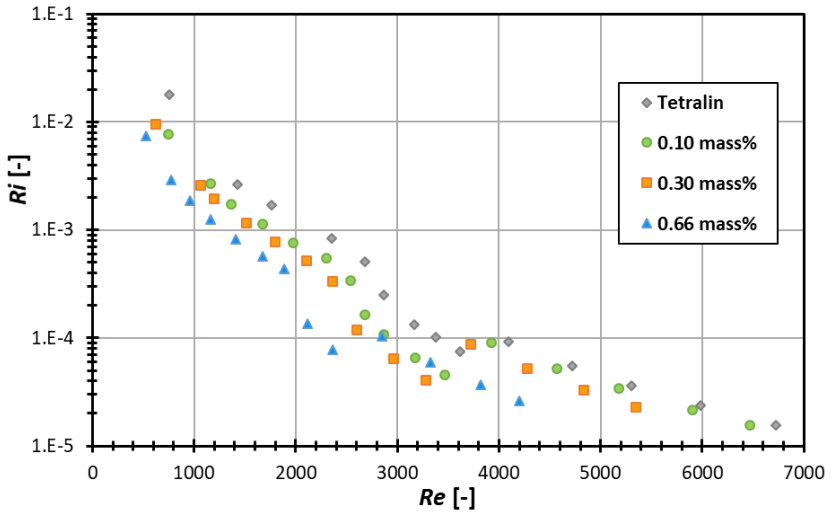

Figure 4.4: Richardson number versus Reynolds number as a function of nanoparticles mass fraction, at $T_i = 45$°C.

It is easy to see that for all cases the Richardson number is smaller than 0.1, meaning that only forced convection is present in the flow.

4.4 Thermal losses

As explained in 3.1 the experimental setup allows to apply an imposed and fixed heat power and there for a heat flux value (q_s'') to the test section. This thermal power, q_{imp} in W, imposed to the tube wall is calculated by:

$$q_{imp} = IV \tag{4.1}$$

where I is the electrical current and V is the voltage provided by the power source. In all the tests performed, the heat transfer rate applied, ranging from a mean value of 10V for laminar/transition flow, up to to 15V for turbulent flow. However, due to thermal losses to the surroundings, the actual heat rate that is transferred to the working fluid is less than the imposed one. An energy balance to a control volume for the internal flow in the tube gives:

$$q_{real} = \dot{m}Cp(\Delta T) \tag{4.2}$$

where ΔT represents the difference between inlet and outlet temperatures, as in the equation 2.14. The thermal efficiency is given by:

$$\eta = \frac{q_{real}}{q_{imp}} \tag{4.3}$$

(a)

	Thermal efficiency [%]		
Re	25°C	35°C	45°C
≈1300	85.69	83.83	81.63
≈2500	89.52	86.52	85.28
≈5000	91.61	90.38	90.56

(b)

	Thermal efficiency [%]			
Re	Tetralin	0.10%	0.30%	0.66%
≈1400	85.52	85.69	86.59	87.68
≈2400	86.62	88.32	90.69	92.08
≈5000	90.74	91.61	91.89	95.46

Table 4.1: Thermal efficiency obtained for the working fluids at different experimental conditions: (a) thermal efficiency obtained for the 0.10 mass% nanofluid at different flow regimes and inlet temperatures (b) thermal efficiency of all the working fluids at different flow regimes for $T_i = 25$°C.

The results show that for all the cases the efficiency increases as the Reynolds number increases tending to stabilize in the turbulent flow. However, as the temperature increases the efficiency tends to decrease, specially in the laminar flow. This trend is clear in table 4.1(a) which presents the thermal efficiency for 0.10 mass% nanofluid at the three different temperatures tested and for specific Reynolds numbers taken in each flow regime. This reduction of the efficiency is easily explained by equation 2.15, since as the temperature raises the specific heat capacity increases and the difference between the inlet and outlet temperatures (ΔT) will decrease. On the other hand, as the temperature increases the density decreases and the mass flow rate, for the same Reynolds number, have to decrease, which causes a reduction of the actual heat rate that is transfer to the working fluid (q_{real}). Also, the efficiency tends to increase as the concentration of the nanofluid increases. Results for an inlet temperature of 25°C are presented in figure 4.5 and in table 4.1(b), being the maximum thermal efficiency obtained

of 95.46% for 0.66 mass% nanofluid at 25ºC. The lowest thermal efficiency obtained was 79.55% for pure tetralin at 45ºC, for a Reynolds value of 755 (laminar flow). As well as the explanation for the temperature raise, with the raise in mass particles, the specific heat capacity slightly decreases, and for the same Reynolds number, as the density increases with mass concentration, the mass flow rate has to increase. This will cause an increase of the efficiency that is not cause by the specific heat capacity, as expected, but by the other thermophysical properties of the nanofluid, namely, the viscosity and the density.

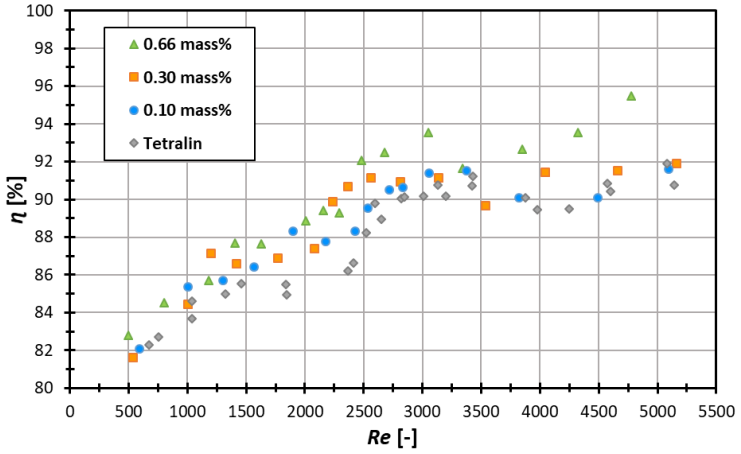

Figure 4.5: Thermal efficiency versus Reynolds number as a function of nanoparticles mass fraction, at $T_i = 25$ºC.

4.5 Hydrodynamic characteristics.

4.5.1 Pressure drop

As previously explained in section 2.2.1, the pressure drop is an important factor when analyzing an internal flow since it directly affects the required pumping power. Since the viscosity of the nanofluids increases with the nanoparticles mass fraction (3.3.1), the pressure drop is larger for an increased concentration of the nanoparticles. This pressure drop increase observed for the nanofluids, when compared to the flow of pure tetralin, is quite clear in figures 4.6, becoming more significant at larger inlet temperatures. This trend can be related to the viscosity of the fluids, since the viscosity decrease with the temperature is not exactly the same for all the nanofluids tested. In fact, figure 3.7 shows a divergence between the curves of tetralin and nanofluids with lower nanoparticles concentration and the nanofluid with the largest nanoparticles concentration which shows an overall larger viscosity, that tends to decrease less with temperature.

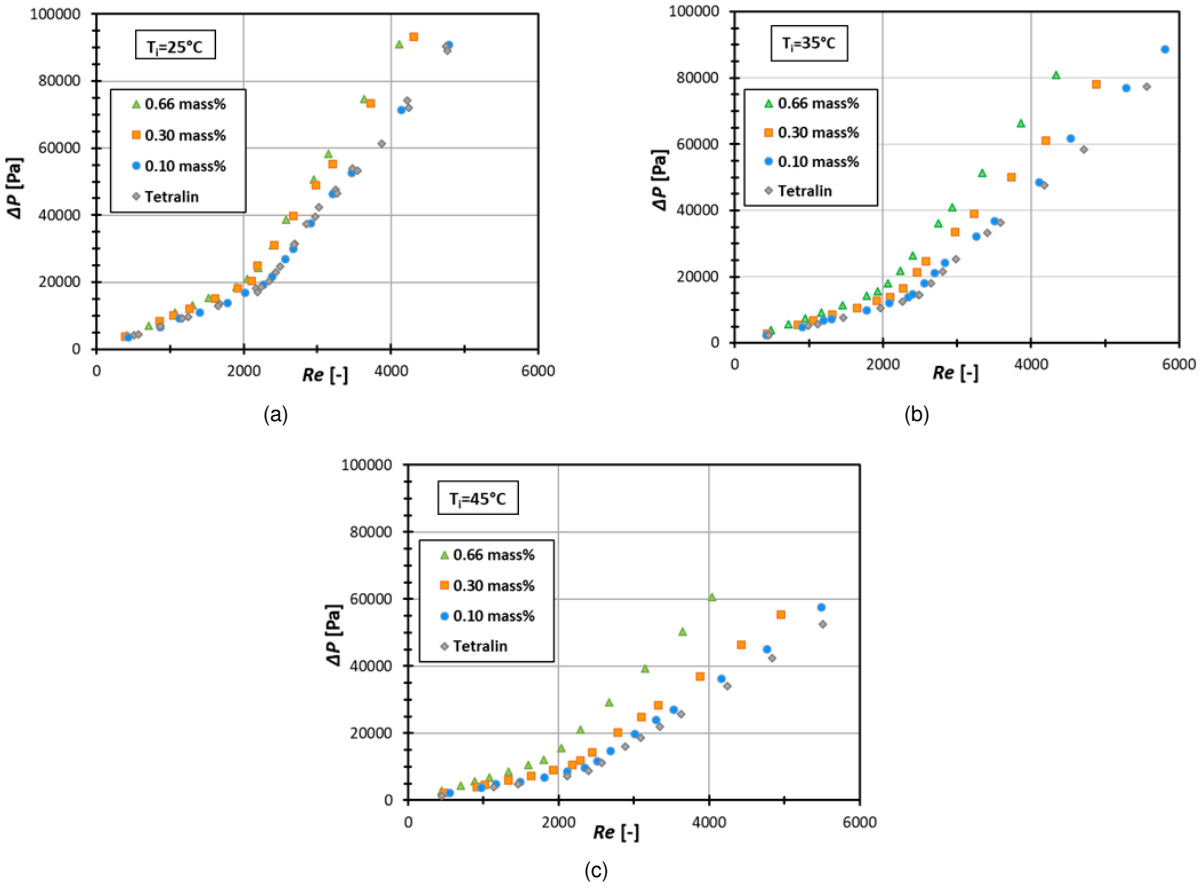

Figure 4.6: Pressure drop versus Reynolds number as a function of nanoparticles mass fraction for T_i of (a) 25ºC (b) 35ºC (c) 45ºC.

4.5.2 Friction factor

Evaluating the friction factor, as depicted in figures 4.7 for 0.10 mass%, 0.30 mass%, 0.66 mass% C_{60}/tetralin nanofluids and pure tetralin, the difference between the nanofluids and the tetralin is almost negligible, both in the laminar and in the turbulent regime. The experimental results are compared with Hagen-Poiseuille and Blasius equations, depicting a very good agreement. Analyzing the figures with more detail, it is possible to notice that, in the laminar flow regime, the friction factor does not depend of the particles concentration, being the values of the friction factor versus Reynolds number the same as for pure tetralin. The largest difference obtained between the nanofluids and tetralin was about 4% for an inlet temperature of 45ºC.

The difference in the friction factor between the nanofluids and the tetralin is slightly larger in the turbulent flow, particularly as the inlet temperature and the nanoparticles concentration increases. Hence, the largest values of the friction factor were obtained for the 0.66 mass% nanofluid, at 45ºC, which was observed to be about 8.8% larger, for a Reynolds number of 3600, when compared to that of tetralin. This trend can be explained by the viscosity of the nanofluids, as discussed in the previous paragraphs. However, since as the temperature increases, the dynamic viscosity of the fluids decrease and the difference between them becomes more significant, specially for 0.66 mass% nanofluid, and, since the difference between the density of the nanofluids, figure 3.5, remains constant with temperature raise, it

is possible to conclude that with temperature augmentation, the friction factor will increase with nanoparticles concentration, when compared to that of pure tetralin. At the same time, the Reynolds number, for the same fluid velocity, will be higher for tetralin and for the nanofluids with lower mass concentration. So, the transition from laminar to turbulent seems to occur at lower Reynolds for the nanofluid with larger concentration (even though that may not be true) and its friction factor values will increase. So, overall one can observe that the friction factor increases with mass concentration of nanoparticles augmentation, being this more pronounced as the temperature increases.These differences are also more prominent in transition and turbulent regimes, which are more affected by viscous and mixture effects.

This analysis reveals that, as the temperature increases, an increase of the mass nanoparticles will cause extra penalty in pumping power when compared to pure tetralin.

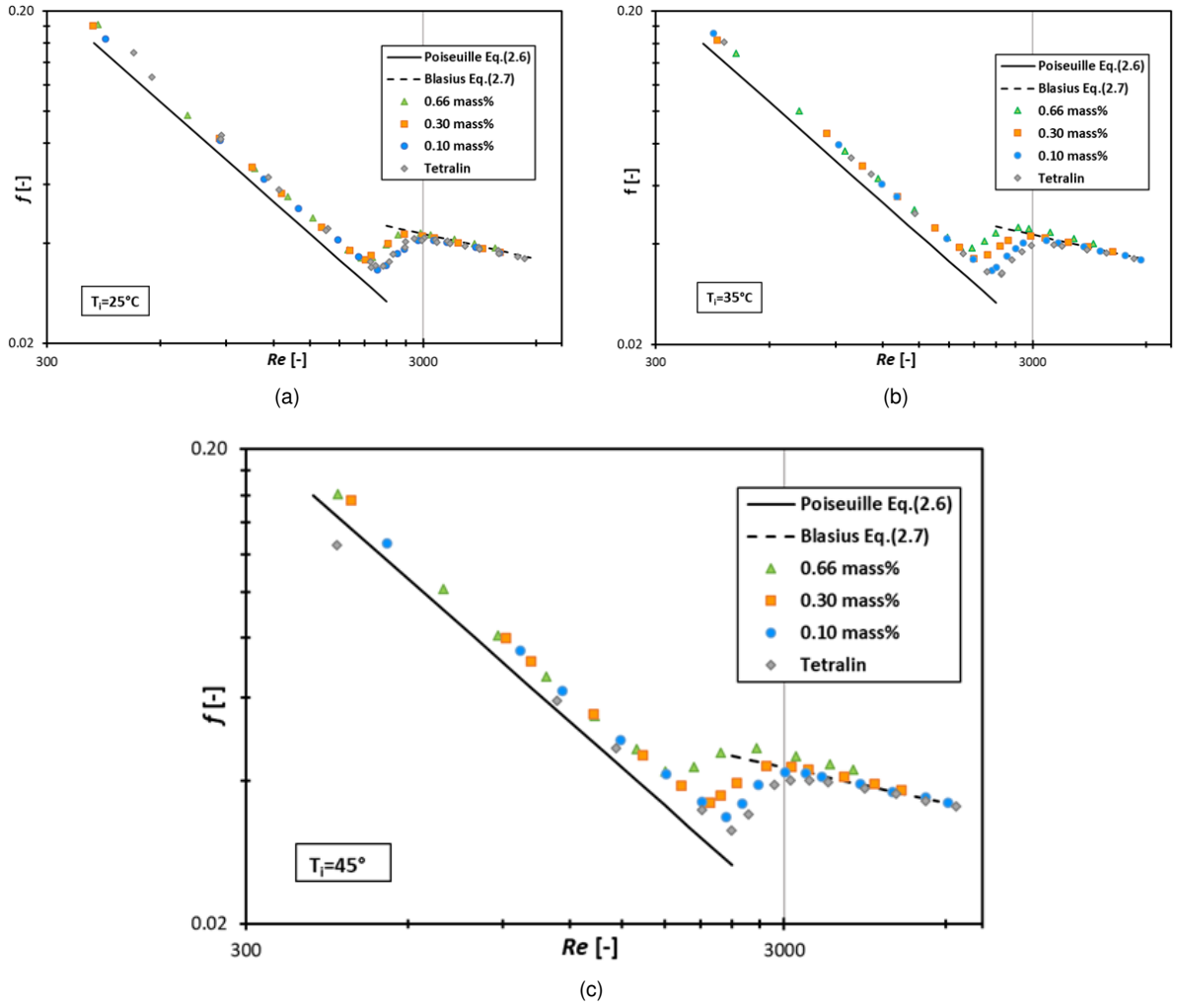

Figure 4.7: Friction factor versus Reynolds number as a function of nanoparticles mass fraction for T_i of (a) 25°C (b) 35°C (c) 45°C.

As aforementioned, the results also suggest an early transition to the turbulent flow for nanofluids, being this transition as early as the increase of mass concentration of the nanofluid. These results are consistent with those observed in the pressure drop. However, a more detailed analysis is required, also looking at the heat transfer results (as discussed later in this thesis) given the variation in the Reynolds number, that is associated to the difference between the viscosity, at different temperatures, that is

observed for the different nanoparticles concentrations.

4.6 Heat transfer

4.6.1 Convective heat transfer coefficient

The experimental values obtained for the heat transfer coefficient, as a function of the Reynolds number are depicted for an inlet temperature of 45ºC in figure 4.8 (b). Figure 4.8 (a) shows a particular set of results, focusing just on the heat transfer coefficients obtained in the laminar flow regime, at an inlet temperature of 25ºC. The results reveal that in the laminar region the heat transfer coefficient is not affected by the addition of the nanoparticles, having just a slight increase as the Reynolds number increases. However, in the turbulent region, the heat transfer coefficient increases with the mass concentration of nanoparticles. This augmentation is more pronounced as the temperature increases (this is why the results depicted in figure 4.8 (b) were selected for the highest inlet temperature tested). For turbulent flow, at a Reynolds number of approximately 4000, the heat transfer coefficient is enhanced by 4.9% when using 0.10 mass% nanofluid, by 11.2% when using 0.30 mass% and 30.5% when using 0.66 mass% nanofluid.

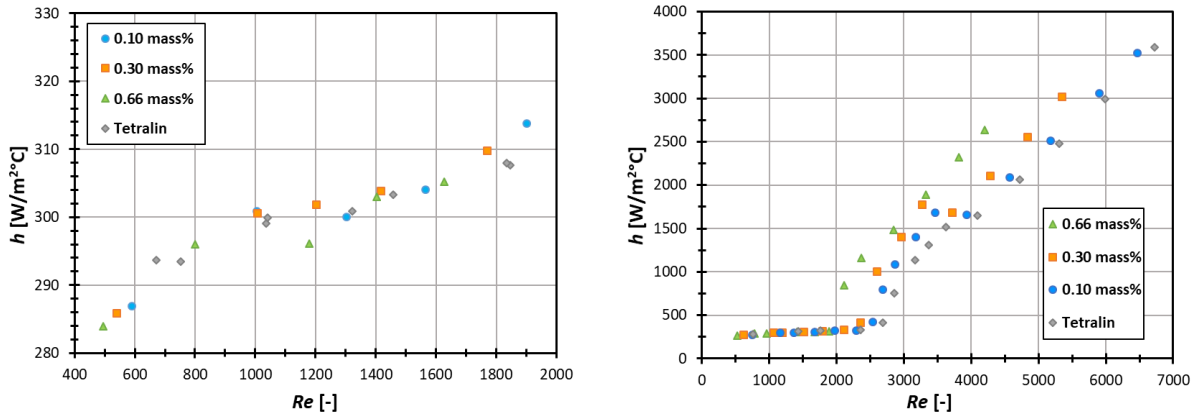

Figure 4.8: Heat transfer coefficient versus Reynolds number as a function of nanoparticles mass fraction at (a) $T_i = 25$ºC for laminar region (b) $T_i = 45$ºC.

However, looking at the evolution of the heat transfer coefficient as a function of the Reynolds number can be deceiving when comparing the different nanofluids, since, as discussed in previous points, the viscosity varies in a different way on temperature, depending on the nanoparticles concentration, which may alter the values of the Reynolds number in a way that disables an accurate comparison between the different fluids. Hence, as an alternative, earlier proposed by Pak and Cho [56] and also implemented by Meyer et al. [34] the heat transfer coefficients obtained for the various fluids are compared in figure 4.9 under the condition of constant average velocity. The results show that for a mean velocity value

of 1.5 m/s, the heat transfer coefficient of 0.10 mass% C_{60}/tetralin nanofluid is 1.22% higher, at 0,30 mass% is 2.06% higher and at 0.66 mass% is 8.36% lower than pure tetralin. This slight decrease of the convective heat transfer coefficient can be appreciated in figure 4.9 and is only observed in the turbulent flow regime.

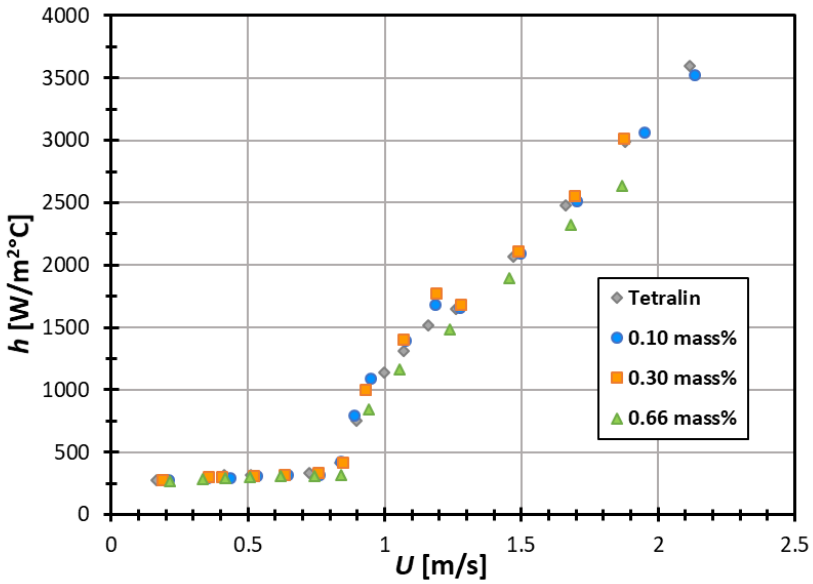

Figure 4.9: Heat transfer coefficient versus mean fluid velocity as a function of nanoparticles mass fraction, at $T_i = 45$°C.

This decrease of the heat transfer coefficient for the nanofluid with the highest concentration tested, can be explained by the findings reported by Rudyak et al. [73], who studied the transition (from laminar to turbulent regime) of a nanofluid flow inside a pipe. Rudyak et al. [73] observed that, with increasing concentration of nanoparticles, the transition occurred at smaller Reynolds numbers. However, Rudyak et al. [73] also measured the pressure pulsations in the tube and observed that in turbulent flow regime, the nanoparticles reduce the pressure pulsations. This reduction leads to a decrease of the small-scale turbulent fluctuations, i.e, a turbulence degree reduction, decreasing the mixing inside the pipe, which results in lower heat transfer coefficient.

4.6.2 Nusselt number

Nusselt number was also evaluated for the four fluids at the three different inlet temperatures. As expected, and in agreement with the results discussed in subsection 4.6.1, due to equation 2.17, for the same Reynolds number, as the mass concentration of the nanofluid increases, the Nusselt number also increases, being this increase more significant at the highest temperature tested, 45°C, as can be seen in figure 4.10. The results show a raise of the Nusselt number of about 56% for 0.66 mass% nanofluid, at a Reynolds number of about 4100. However, this augmentation only affects the turbulent region, not affecting the laminar region neither by the temperature or the particles concentration.

Heat transfer results were compared to the correlations proposed by Meyer et al. [42], presented in section 2.1.2 and depicted in table 2.1. For the conditions used here, equation E, with equation D for

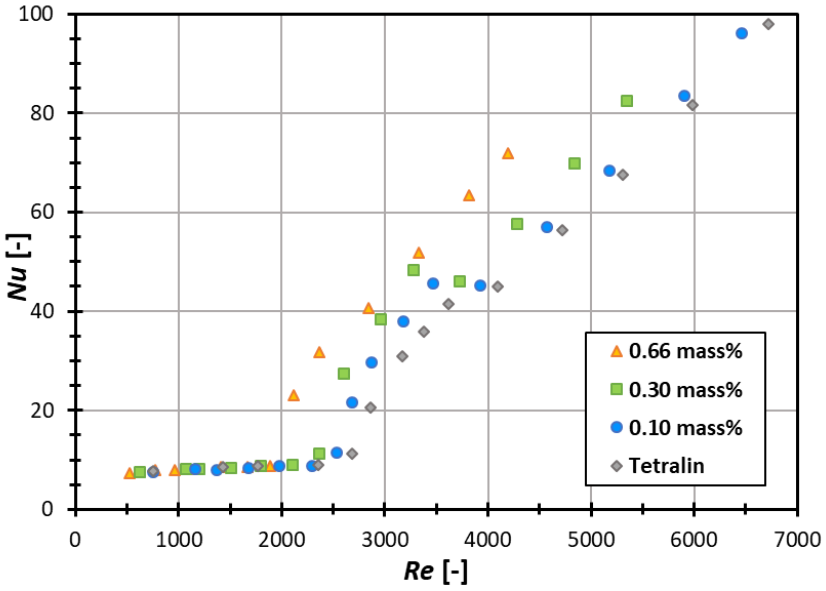

Figure 4.10: Nusselt number versus Reynolds number as a function of nanoparticles mass fraction, at $T_i = 45$°C.

quasi-turbulent and turbulent flow were used.

As the temperature increases, the experimental data tends to deviate from the correlation, as observed in figure 4.11 (a).

For the lowest inlet temperature tested, the correlation predicts values close to the experimental ones for laminar and turbulent flow regimes, as shown in figure 4.11 (b). This good agreement between the correlation and the experimental values is particularly evident for tetralin and 0.10 mass% nanofluid. However, the correlation overpredicts the experimental data in the transition flow regime, being obtained a major deviation of about 70% for tetralin.

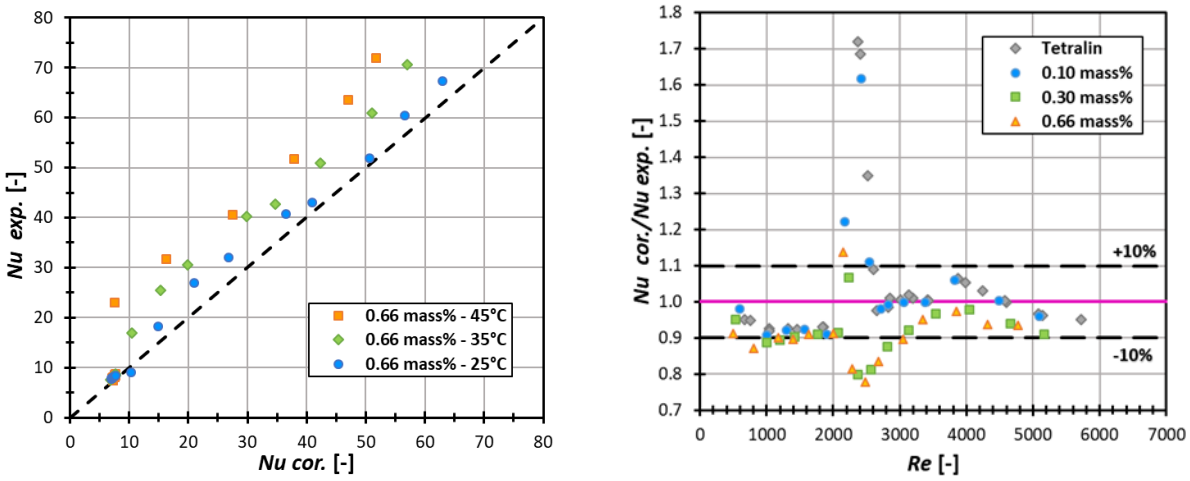

(a) (b)

Figure 4.11: Deviation between the experimental Nusselt number and equation E (a) for 0.66 mass% nanofluid (b) versus Reynolds number for tetralin and nanofluids at $T_i = 25$°C.

For 0.30% and 0.66 mass% nanofluids the correlation tends to underpredict the experimental values.

The maximum deviation between the experimental data and the correlation is also obtained in the transition flow regime, for a Reynolds number of 2481 (the deviation is -22.3%). The average deviation for tetralin and the three nanofluids is presented in the next table, 4.2, for laminar flow regime, considering $Re < 2000$, for turbulent flow regime, $Re > 3000$, and for the total range. It can be concluded that, from table 2.1, equation A and D predict well the experimental Nusselt number for laminar and turbulent flow regime, respectively. However the equation for the transitional flow regime, equation B is not so suitable for the fluids and working conditions tested here. The accurate description of the heat transfer processes occurring for the nanofluids tested here requires a much deeper investigation, to be developed in a future work. However, the deviation between the relations reported in the literature and the experimental data can be related to the fact that these correlations are not capturing well the relation between the variation of the physical properties of the nanofluids (e.g. the viscosity) and the concentration of the particles, which in turn will affect the flow.

	Laminar	Turbulent	Total
Tetralin	-6.78	0.65%	4.82%
0.10 mass%	-7.08%	0.47%	3.95%
0.30 mass%	-9.08%	-5.68%	-8.45%
0.66 mass%	-10.15%	-6.13%	-8.92%

Table 4.2: Average deviation between experimental Nusselt number and equation E, at $T_i = 25$ºC.

4.6.3 Colburn j-factor

Considering the subjective determination of the transition region based on the visual inspection of the plots (e.g. of the friction factor as a function of the Reynolds number) and taking into account the complex effects that the variation in the nanofluids properties such as the viscosity play on the flow and on the calculation of the Reynolds number, depending on the inlet temperature and on the mass concentration of the nanoparticles, the Colburn j-factor was used as a complementary parameter, as proposed by Everts and Meyer [43].

Looking at the Colburn j-factor, as a function of the Reynolds number and in agreement with the results discussed in the previous sections, the transition from laminar to turbulent occurs at lower Reynolds numbers, as the mass concentration of C_{60} nanoparticles increases, as can be seen in figure 4.12. This trend is more pronounced for higher inlet temperatures. Although these results can be clearly seen in the graphics that have been presented, again care must be taken in their interpretation which is still based on the visual inspection of plots presented as a function of the Reynolds number. Aiming at a more accurate identification of the critical conditions for the occurrence of the transition, the Colburn j-factor gradient as a function of the Reynolds number is evaluated as given in equation 2.19, following the method proposed by Everts and Meyer [43]. Figure 4.13 shows, as an illustrative example, the obtained Colburn j-factor gradient as a function of the Reynolds number for 0.10 mass% nanofluid for the three inlet temperatures tested.

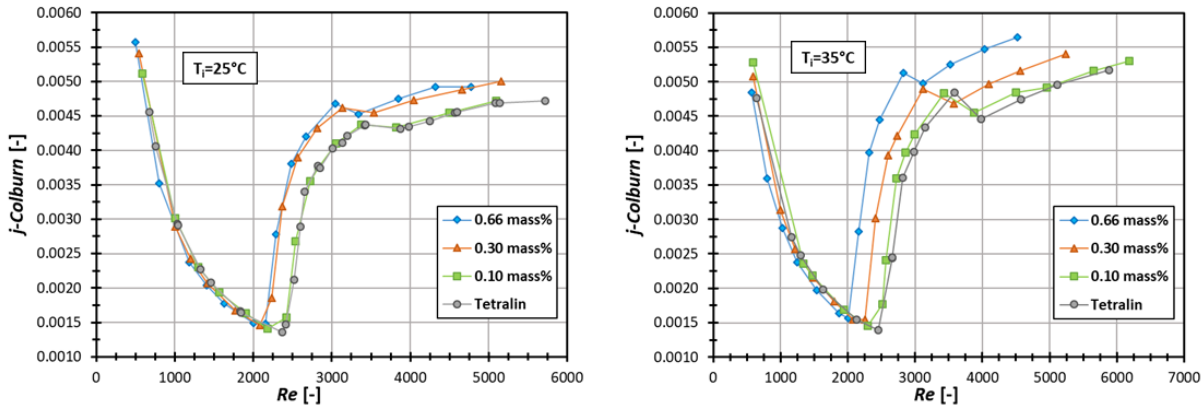

(a)

(b)

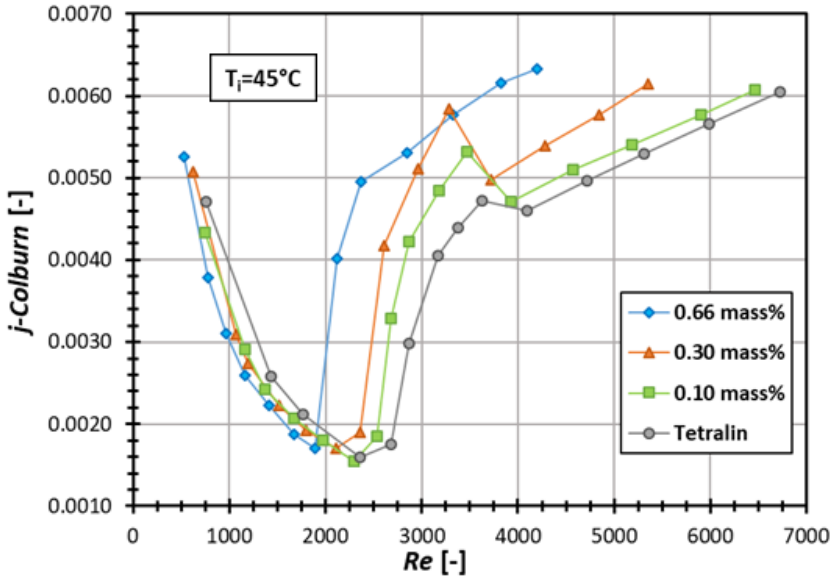

(c)

Figure 4.12: Colburn j-factor as a function of Reynolds number, at T_i of (a) 25°C (b) 35°C (c) 45°C.

The closest value as possible of the critical Reynolds, Re_{crt}, i.e. the Reynolds for the start of the transition flow regime and end of the laminar flow regime, was obtained as the derivative turns from negative to positive. The obtained values, for tetralin, 0.10%, 0.30% and 0.66 mass% nanofluids at the three different inlet temperatures are summarized in table 4.3.

	25°C	35°C	45°C
Tetralin	2388	2469	2570
0.10 mass%	2315	2363	2389
0.30 mass%	2113	2253	2231
0.66 mass%	2155	2017	1902

Table 4.3: Critical Reynolds number.

The results clearly show a decrease of the critical Reynolds number as the nanoparticles mass concentration increases, for all the temperatures tested. This corroborates the previously obtained results

discussed when analyzing the pressure drop, the friction factor, the heat transfer coefficient and Nusselt number, of the transition to occur earlier, i.e. at lower Reynolds numbers for the nanofluids, being this as early as the mass fraction of nanoparticles increases.

On the other hand, it is possible to see a general increase of the critical Reynolds number as the temperature increases, i.e, an overall delay in transition, as the temperature increases. Although, for the nanofluid with the highest concentration, 0.66 mass%, the transition starts earlier as the temperature increases. This anticipation of the transition with the temperature raise can be explained again with the dynamic viscosity, following the same arguments used in 4.5.2.

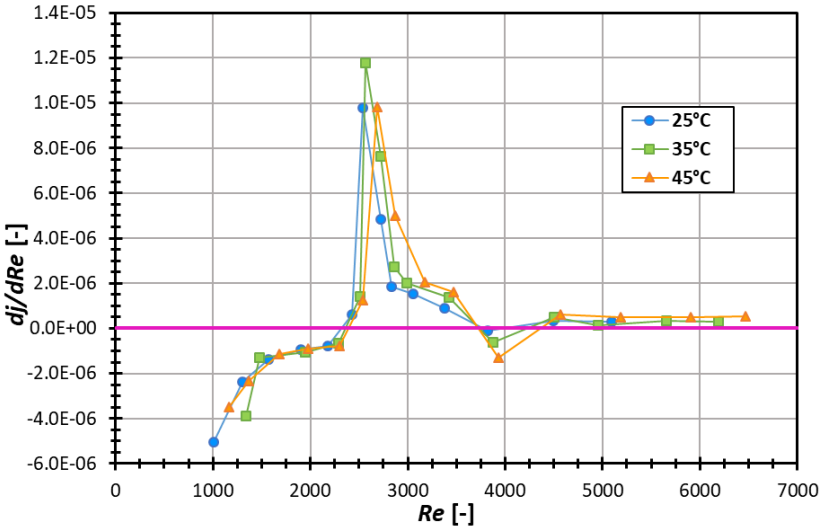

Figure 4.13: Colburn j-factor gradient versus Reynolds number, as a function of the inlet temperature for 0.10 mass% nanofluid.

In the following figure, 4.14, the results of the friction factor as a function of the inlet temperature for the three nanofluids are presented. In each figure the critical Reynolds number values shown in table 4.3 are clearly defined, for the lower and higher temperatures tested. As can be seen, the critical Reynolds numbers obtained with this method, clearly match with those pointed when discussing the friction factor results, thus corroborating the trends presented in this thesis.

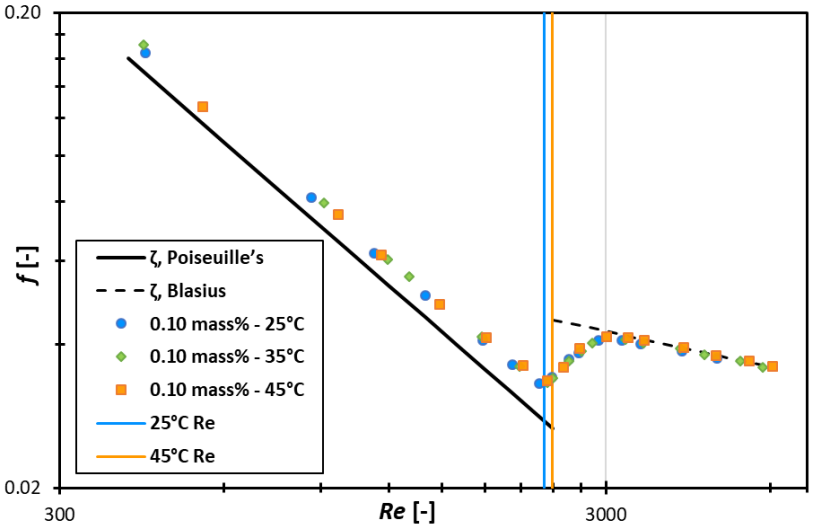

(a)

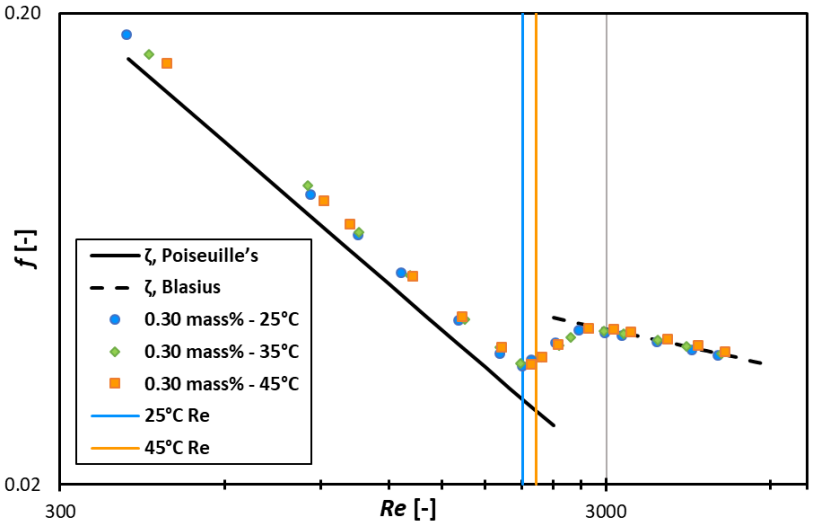

(b)

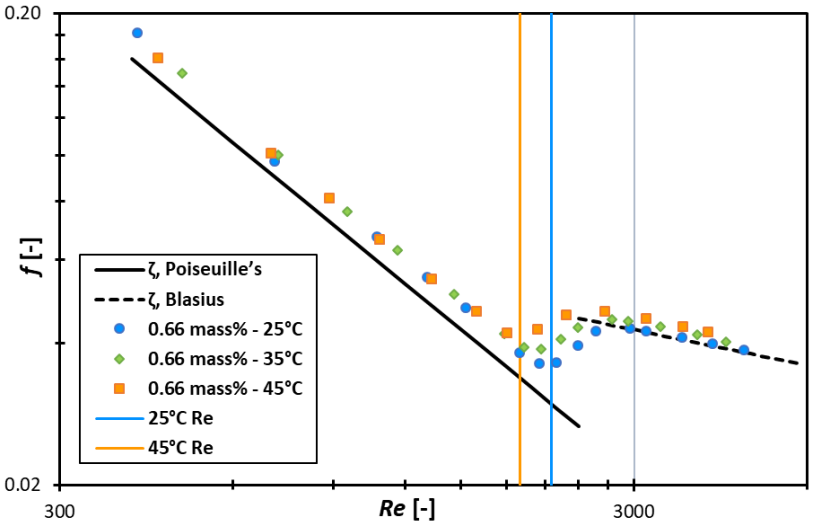

(c)

Figure 4.14: Friction factor versus Reynolds number as a function of the inlet temperatures for (a) 0.10 mass% (b) 0.30 mass% (c) 0.66 mass%.

Chapter 5

Conclusions

5.1 Summary

The present work was aimed at evaluating the potential benefits of using C_{60}/tetralin nanofluid as a working fluid for a heat exchanger to enhance the heat transfer mechanisms. So, this thesis presents a study on the effects of adding fullerene nanoparticles on the heat transfer and hydrodynamic behavior on C_{60}/tetralin nanofluid flowing inside a horizontal, circular and smooth tube with a constant heat flux applied. Particular emphasis is given to the effect of increasing the mass concentration of the particles and the inlet temperature of the working fluid.

First, an analysis to the thermophysical properties of the nanofluids was performed. The effect of the mass concentration and inlet temperature increase in each property is summarized in table 5.1.

Properties	Temperature ↑	Mass concentration ↑
Density, ρ	↓	↑
Viscosity, μ	↓	↑
Thermal conductivity, k	↓	×
Specific heat, Cp	↑	↓

Table 5.1: Relation of thermophysical properties with temperature and mass concentration.

Analyzing the flow of the various working fluids it was concluded that regardless the working fluid, the flow was hydrodynamically fully developed for all the Reynolds numbers range, being therefore independent from the mass concentration and inlet temperature. However, when studying the thermal entry length, it was concluded that for turbulent flow regime, the flow was thermally developed, but, for laminar regime, the flow was developing.

An evaluation of the Richardson number showed that only forced convection was present in the flow for all the fluids and all the conditions tested. Regarding the thermal losses, the thermal efficiency tends to increase with mass concentration of C_{60} nanoparticles as well with the Reynolds number, being higher in the turbulent flow regime. Furthermore the thermal efficiency tends to decrease with the inlet temperature augmentation. This was justified not by the specific heat capacity but by the viscosity of the

nanofluids.

The general results show that adding C_{60} to tetralin increases the pressure drop and also the heat transfer coefficient, as well as the Nusselt number, being this augmentation more pronounced with the increase of the inlet temperature of the fluid.

The experimental results showed that, for the friction factor, an increase of the temperature will cause a friction factor raise, in the laminar flow regime, of the nanofluids in relation with tetralin. Also, a friction factor raise is observed in the turbulent regime, which is more pronounced as the mass concentration of the nanoparticles increase. This represents a pumping power penalty when using the nanofluids, more significant with the concentration of C_{60} nanoparticles and, also, the temperature raise. This results were justified by the viscosity variation with temperature, since as the temperature increases, the difference between the dynamic viscosity of the fluids becomes more significant, specially for 0.66 mass% nanofluid.

When analyzing the effect of the nanoparticles on the convective heat transfer coefficient the results depend on the method to do it. A first analysis showed an increase of the heat transfer with the increasing values of the Reynolds number, for the transitional and turbulent flow regime, almost not being affected in the laminar flow regime, reaching this increase about 30.5%, in the turbulent flow, when using 0.66 mass% nanofluid. However, when comparing the heat transfer coefficient of the various fluids as a function of the mean velocity of the flow, the nanofluid with the highest concentration showed a decrease of about 8.36% when compared to pure tetralin, being this decrease of the heat transfer coefficient attributed to the reduction in the degree of turbulence.

Studying the Colburn j-factor and its gradient as a function of Reynolds number made possible to better evaluate the start of the transition flow regime. The results obtained show an earlier transition (i.e. occurring at a lower Reynolds number). When assessing the influence of the inlet temperature in the transition, the results show a delay in the laminar-turbulent transition with temperature raise, except for the nanofluid with highest concentration. For 0.66 mass% nanofluid the opposite trend is observed which is explained by the dynamic viscosity of the nanofluid.

Using different methods to identify the occurrence of transition allowed to confirm the consistency of the trends evaluated in each method, stressing that the major role of the nanoparticles concentration, for the range studied in the present work, was to alter relevant bulk properties of the fluids, namely the viscosity, which dominated over the variation of other properties such as the thermal conductivity. Overall these effects became dominant leading to a significant increase of the heat transfer coefficient despite of the penalty in the pumping power. So, the use of this nanofluid is recommended as a working fluid with enhanced thermal properties, although the concentration of the nanoparticles should be carefully considered due to the increase pumping power penalty and the deterioration of the heat transfer coefficient for concentration equal or higher than 0.66 mass%.

5.2 Future Work

After the conclusion of this study, a few ideas for future work with C_{60}/tetralin nanofluid are suggested.

A better characterization of the nanofluids thermophysical characteristics, in particular, the thermal conductivity property. The measurement of this property with a more sensible procedure will allow a better identification of the effects of the C_{60} nanoparticles addiction in the fluid.

A more detailed study of this nanofluid in the transition flow regime, to better evaluate its behavior under this flow condition and to assess the possible use of this nanofluid as a working fluid on a heat exchanger operating in the conditions studied here.

The study of this nanofluid inside corrugated tubes or other kind of enhanced tube, such as, tubes with internal integrated fins or twisted tapes is also interesting to explore, with the goal of evaluating the possible use of C_{60}/tetralin in this type of pipes.

Finally study the effect of the nanoparticles addition on the surface wettability and its influence in the heat transfer is also a topic of interest for future work.

Bibliography

[1] H. Santos, D. Caseiro, N. Pires, J. F. Pereira, J. Morgado, and N. Martinho. Experimental Study of an Evaporator Heat Exchanger for a Rankine Cycle Vehicle Waste Heat Recovery System. *Journal of Clean Energy Technologies*, 4(5):362–366, 2015.

[2] H. Santos, J. Morgado, N. Martinho, J. Pereira, and A. Moita. Selecting and Optimizing a Heat Exchanger for Automotive Vehicle Rankine Cycle Waste Heat Recovery Systems. *Energy Procedia*, 107(September 2016):390–397, 2016.

[3] H. Santos, A. Domingues, and M. Costa. Analysis of vehicle exhaust waste heat recovery potential using a Rankine cycle. *Energy*, 49(1):71–85, 2013.

[4] F. A. Andrade. Caracterização Experimental da Transmissão de Calor em Escoamentos no Interior de Tubos Corrugados. Dissertação de Mestrado em Engenharia Mecânica: Instituto Superior Técnico, 2018.

[5] Y. Li, J. Zhou, S. Tung, E. Schneider, and S. Xi. A review on development of nanofluid preparation and characterization. *Powder Technology*, 196(2):89–101, 2009.

[6] M. U. Sajid and H. M. Ali. Recent advances in application of nanofluids in heat transfer devices: A critical review. *Renewable and Sustainable Energy Reviews*, 103:556–592, 2019.

[7] S. M. S. Murshed, K. C. Leong, C. Yang, and N.-T. Nguyen. Convective heat transfer characteristics of aqueous TiO2 nanofluid under laminar flow conditions. *International Journal of Nanoscience*, 07 (06):325–331, 2009.

[8] Q. Li and Y. Xuan. Convective heat transfer and flow characteristics of Cu-water nanofluid. *SCIENCE IN CHINA (Series E)*, 45(4):408–416, 2002.

[9] R. Saidur, K. Y. Leong, and H. A. Mohammad. A review on applications and challenges of nanofluids. *Renewable and Sustainable Energy Reviews*, 15(3):1646–1668, 2011.

[10] M. U. Siddiqui, O. K. Siddiqui, A. Al-sarkhi, A. F. M. Arif, and S. M. Zubair. A novel heat exchanger design procedure for photovoltaic panel cooling application : An analytical and experimental evaluation. *Applied Energy*, 239(October 2018):41–56, 2019.

[11] A. R. Ã, C. J. Dey, and D. R. Mills. Cooling of photovoltaic cells under concentrated illumination : a critical review. *Solar Energy Materials & Solar Cells*, 86(2005):451–483, 2006.

[12] M. A. Farahat. Improvement the thermal electric performance of a photovoltaic cells by cooling and concentration techniques. In *39th International Universities Power Engineering Conference, UPEC 2004 - Conference Proceedings*, volume 2, pages 623–628, 2004.

[13] A. Akbarzadeh and T. Wadowski. Heat pipe-based cooling systems for photovoltaic cells under concentrated solar radiation. *Applied Thermal Engineering*, 16(1):81–87, 1996.

[14] S. Odeh and M. Behnia. Improving photovoltaic module efficiency using water cooling. *Heat Transfer Engineering*, 30(6):499–505, 2009.

[15] M. Alobaid, B. Hughes, D. O. Connor, J. Calautit, and A. Heyes. Improving Thermal and Electrical Efficiency in Photovoltaic Thermal Systems for Sustainable Cooling System Integration. *Journal of Sustainable Development of Energy, Water and Environment Systems*, 6:305–322, 2018.

[16] A. Kasaeian, A. T. Eshghi, and M. Sameti. A review on the applications of nanofluids in solar energy systems. *Renewable and Sustainable Energy Reviews*, 43:584–598, 2015.

[17] A. Wahab, A. Hassan, M. Arslan, H. Babar, and M. Usman. Solar energy systems – Potential of nanofluids. *Journal of Molecular Liquids*, 289, 2019.

[18] H. W. Kroto, J. R. Heath, S. C. O'Brien, R. F. Curl, and R. E. Smalley. C60 : Buckminsterfullerene. *Letters to nature*, 318:162–163, 1985.

[19] M. Dresselhaus, G. Dresselhaus, and P. Eklund. *Science of fullerenes and carbon nanotubes*. Academic Press, 1996.

[20] A. Martin and M. M. Bou-Ali. Determination of thermal diffusion coefficient of nanofluid: Fullerene-toluene. *Comptes Rendus - Mecanique*, 339(5):329–334, 2011.

[21] R. Ruoff. Solubility of C60 in a variety of solvents. *J. Phys. Chem.*, 97:3379–3383, 1993.

[22] P. Rautanen, M. Lylykangas, J. Aittamaa, and A. Krause. Liquid Phase Hydrogenation of Naphthalene on Ni/Al2O3. *Reaction Kinetics and the Development and Operation of Catalytic Processes*, 133:309–316, 2007.

[23] P. N. Kuznetsov, E. D. Korniyets, C. E. Snape, J. Bimer, L. I. Kuznetsova, and P. D. Salbut. The nature of the synergistic effect of binary tetralin-alcohol solvents in Kansk-Achinsk brown coal liquefaction. *Fuel Processing Technology*, 50(2-3):139–152, 2002.

[24] L. Li, Y. Hou, W. Wu, S. Liang, and S. Ren. Behaviors of tetralin and 9,10-dihydroanthracene as hydrogen donor solvents in the hydrogenolysis of coal-related model compounds. *Fuel Processing Technology*, 191(March):202–210, 2019.

[25] K. M. Isa, T. A. T. Abdullah, and U. F. M. Ali. Hydrogen donor solvents in liquefaction of biomass: A review. *Renewable and Sustainable Energy Reviews*, 81(April 2017):1259–1268, 2018.

[26] Pharmacompass.com. URL `https://www.pharmacompass.com/price/tetralin`. Last accessed 11/10/2019.

[27] Y. Chikazawa, M. Farmer, and C. Grandy. Technology Gap Analysis on Sodium-Cooled Reactor Fuel-Handling System Supporting Advanced Burner Reactor Development. *Nuclear Technology*, 165(3):270–292, 2017.

[28] A. V. Kozlov, A. M. Kolker, N. G. Manin, and N. I. Islamova. Polythermal study of C60 solubility in tetralin. *Mendeleev Communications*, 17(6):362–363, 2007.

[29] J. Meyer and J. Olivier. Heat Transfer in tubes in the Transitional Flow Regime. In *Evaporation, Condensation and Heat transfer*. 2014.

[30] F. P. Incropera, A. S. Lavine, T. L. Bergman, and D. P. DeWitt. *Fundamentals of heat and mass transfer*. Wiley, 2007.

[31] J. P. Meyer and J. A. Olivier. Heat transfer and pressure drop characteristics of smooth horizontal tubes in the transitional flow regime. *Heat Transfer Engineering*, 35(14-15):1246–1253, 2014.

[32] J. Meyer and J. Olivier. Heat Transfer of developing flow in the Transitional Flow Regime. *Evaporation, Condensation and Heat transfer*, pages 1–13, 2015.

[33] J. P. Meyer, L. Liebenberg, and J. A. Olivier. Single-phase heat transfer and pressure drop of water cooled inside horizontal smooth tubes in the transitional flow regime. *2010 14th International Heat Transfer Conference, IHTC 14*, 2(June 2016):429–436, 2010.

[34] J. P. Meyer, T. J. McKrell, and K. Grote. The influence of multi-walled carbon nanotubes on single-phase heat transfer and pressure drop characteristics in the transitional flow regime of smooth tubes. *International Journal of Heat and Mass Transfer*, 58(1-2):597–609, 2013.

[35] M. Everts, S. R. Ayres, F. A. Mulock Houwer, C. P. Vanderwagen, N. M. Kotze, and J. P. Meyer. The influence of surface roughness on heat transfer in the transitional flow regime. *Proceedings of the 15th International Heat Transfer Conference, IHTC 2014*, pages 1–12, 2014.

[36] J. P. Meyer and S. M. Abolarin. Heat transfer and pressure drop in the transitional flow regime for a smooth circular tube with twisted tape inserts and a square-edged inlet. *International Journal of Heat and Mass Transfer*, 117:11–29, 2018.

[37] M. Everts and J. P. Meyer. Relationship between pressure drop and heat transfer of developing and fully developed flow in smooth horizontal circular tubes in the laminar, transitional, quasi-turbulent and turbulent flow regimes. *International Journal of Heat and Mass Transfer*, 117:1231–1250, 2018.

[38] R. L. Shannon and C. A. Depew. Combined Free and Forced Laminar Convection in a Horizontal Tube With Uniform Heat Flux. *Journal of Heat Transfer*, 90(3):353, 1968.

[39] H. A. Mohammed and Y. K. Salman. The effects of different entrance sections lengths and heating on free and forced convective heat transfer inside a horizontal circular tube. *Science Direct*, 34: 769–784, 2007.

[40] D. D. Ndenguma. Heat transfer and pressure drop in annuli with non-uniform internal wall temperatures in the transition flow regime. PHD in Mechanical engineering, Univertity of Pretoria (December), 2017.

[41] J. P. Meyer and M. Everts. Single-phase mixed convection of developing and fully developed flow in smooth horizontal circular tubes in the laminar and transitional flow regimes. *International Journal of Heat and Mass Transfer*, 117:1251–1273, 2017.

[42] J. P. Meyer, M. Everts, N. Coetzee, K. Grote, and M. Steyn. Heat transfer coefficients of laminar, transitional, quasi-turbulent and turbulent flow in circular tubes. *International Communications in Heat and Mass Transfer*, 105:84–106, 2019.

[43] M. Everts and J. P. Meyer. Heat transfer of developing and fully developed flow in smooth horizontal tubes in the transitional flow regime. *International Journal of Heat and Mass Transfer*, 117:1331–1351, 2018.

[44] S. U. S. Choi and J. A. Eastman. Enhancing thermal conductivity of fluids with nanoparticles (No. ANL/MSD/CP–84938; CONF-951135–29). *International mechanical engineering congress and exhibition*, (March), 1995.

[45] J. Sarkar. A critical review on convective heat transfer correlations of nanofluids. *Renewable and Sustainable Energy Reviews*, 15(6):3271–3277, 2011.

[46] T. Ambreen and M. H. Kim. Heat transfer and pressure drop correlations of nanofluids: A state of art review. *Renewable and Sustainable Energy Reviews*, 91(March):564–583, 2018.

[47] L. Godson, B. Raja, D. Mohan Lal, and S. Wongwises. Enhancement of heat transfer using nanofluids-An overview. *Renewable and Sustainable Energy Reviews*, 14(2):629–641, 2010.

[48] N. Sezer, M. A. Atieh, and M. Koç. A comprehensive review on synthesis, stability, thermophysical properties, and characterization of nanofluids. *Powder Technology*, 344:404–431, 2019.

[49] W. H. Azmi, K. V. Sharma, R. Mamat, G. Najafi, and M. S. Mohamad. The enhancement of effective thermal conductivity and effective dynamic viscosity of nanofluids - A review. *Renewable and Sustainable Energy Reviews*, 53:1046–1058, 2016.

[50] C. T. Nguyen, F. Desgranges, G. Roy, N. Galanis, T. Maré, S. Boucher, and H. Angue Mintsa. Temperature and particle-size dependent viscosity data for water-based nanofluids - Hysteresis phenomenon. *International Journal of Heat and Fluid Flow*, 28(6):1492–1506, 2007.

[51] S. M. Murshed, K. C. Leong, and C. Yang. Enhanced thermal conductivity of TiO2 - Water based nanofluids. *International Journal of Thermal Sciences*, 44(4):367–373, 2005.

[52] M. Ghanbarpour, E. Bitaraf Haghigi, and R. Khodabandeh. Thermal properties and rheological behavior of water based Al2O3 nanofluid as a heat transfer fluid. *Experimental Thermal and Fluid Science*, 53:227–235, 2014.

[53] M. P. Beck, Y. Yuan, P. Warrier, and A. S. Teja. The effect of particle size on the thermal conductivity of alumina nanofluids. *Journal of Nanoparticle Research*, 11(5):1129–1136, 2009.

[54] W. Duangthongsuk and S. Wongwises. Measurement of temperature-dependent thermal conductivity and viscosity of TiO2-water nanofluids. *Experimental Thermal and Fluid Science*, 33(4):706–714, 2009.

[55] X.-q. Wang and A. S. Mujumdar. A review on nanofluids - Part II: Experiments and applications. *Brazilian journal of chemical engineeing*, 25(04):631–648, 2008.

[56] B. C. Pak and Y. I. Cho. Hydrodynamic and heat transfer study of dispersed fluids with submicron metallic oxide particles. *Experimental Heat Transfer*, 11(2):151–170, 1998.

[57] Q. Li and Y. Xuan. Investigation on Convective Heat Transfer and Flow Features of Nanofluids. *Journal of Heat Transfer*, 125(1):151, 2003.

[58] S. E. B. Maïga, S. J. Palm, C. T. Nguyen, G. Roy, and N. Galanis. Heat transfer enhancement by using nanofluids in forced convection flows. *International Journal of Heat and Fluid Flow*, 26(4 SPEC. ISS.):530–546, 2005.

[59] S. E. B. Maïga, C. T. Nguyen, N. Galanis, G. Roy, T. Maré, and M. Coqueux. Heat transfer enhancement in turbulent tube flow using Al2O 3 nanoparticle suspension. *International Journal of Numerical Methods for Heat and Fluid Flow*, 16(3):275–292, 2006.

[60] K. B. Anoop, T. Sundararajan, and S. K. Das. Effect of particle size on the convective heat transfer in nanofluid in the developing region. *International Journal of Heat and Mass Transfer*, 52(9-10): 2189–2195, 2009.

[61] R. S. Vajjha, D. K. Das, and D. P. Kulkarni. Development of new correlations for convective heat transfer and friction factor in turbulent regime for nanofluids. *International Journal of Heat and Mass Transfer*, 53(21-22):4607–4618, 2010.

[62] S. Suresh, K. P. Venkitaraj, P. Selvakumar, and M. Chandrasekar. Effect of Al2O3-Cu/water hybrid nanofluid in heat transfer. *Experimental Thermal and Fluid Science*, 38:54–60, 2012.

[63] A. Moghadassi, E. Ghomi, and F. Parvizian. A numerical study of water based Al2O3 and Al2O3-Cu hybrid nanofluid effect on forced convective heat transfer. *International Journal of Thermal Sciences*, 92:50–57, 2015.

[64] S. K. Sharma and S. Mital. Preparation and evaluation of stable nanofluids for heat transfer application : A review. *Experimental Thermal and Fluid Science*, 79:202–212, 2016.

[65] A. Nikulin, A. Moita, A. Moreira, S. Murshed, A. Huminic, Y. Grosu, A. Faik, J. Nieto-Maestre, and O. Khliyeva. Effect of al2o3 nanoparticles on laminar, transient and turbulent flow of isopropyl alcohol. *International Journal of Heat and Mass Transfer*, 130:1032–1044, 2019.

[66] F. A. Gonçalves, K. Hamano, and J. V. Sengers. Density and Viscosity of Tetralin and Trans-Decalin. *International journal of Thermophysics*, 10(4), 1989.

[67] K. D. Antoniadis, G. J. Tertsinidou, M. J. Assael, and W. A. Wakeham. Necessary Conditions for Accurate, Transient Hot-Wire Measurements of the Apparent Thermal Conductivity of Nanofluids are Seldom Satisfied. *International Journal of Thermophysics*, 37(8), 2016.

[68] N. Vargaftik. Handbook of physical properties of liquids and gases - pure substances and mixtures. second edition. *CRC Press*, 1994.

[69] M. M. Tawfik. Experimental studies of nanofluid thermal conductivity enhancement and applications: A review. *Renewable and Sustainable Energy Reviews*, 75:1239–1253, 2017.

[70] V. Zhelezny, O. Khyliyeva, and A. Nikulin. Effect of fullerenes C60 on heat capacty, density, thermal conductivity and viscosity of tetralin. 165, 2019.

[71] V. Zhelezny, I. Motovoy, O. Khliyeva, and N. Lukianov. Thermochimica Acta An influence of Al2 O3 nanoparticles on the caloric properties and parameters of the phase transition of isopropyl alcohol in solid phase. *Thermochimica Acta*, 671(September 2018):170–180, 2019.

[72] B. N. Taylor and C. E. Kuyatt. Guidelines for evaluating and expressing the uncertainty of NIST measurement results, Gaithersburg, MD, U.S. Departmente of Commerce, Technology Administration, National Institute of Standards and Technology. 1994.

[73] V. Y. Rudyak, A. V. Minakov, D. V. Guzey, M. I. Pryazhnikov, and V. A. Zhigarev. On laminar-turbulent transition in nanofluid flows. *Thermophysics and Aeromechanics*, 23(5):773–776, 2016.